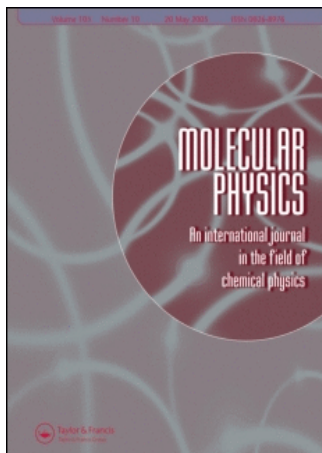


This article was downloaded by:[Ingenta Content Distribution]
On: 7 November 2007
Access Details: [subscription number 768420433]
Publisher: Taylor & Francis
Informa Ltd Registered in England and Wales Registered Number: 1072954
Registered office: Mortimer House, 37-41 Mortimer Street, London W1T 3JH, UK



Molecular Physics

An International Journal in the Field of Chemical Physics

Publication details, including instructions for authors and subscription information:
<http://www.informaworld.com/smpp/title~content=t713395160>

The solvation of sodium ions in water clusters: intermolecular potentials for Na-H₂O and H₂O-H₂O

Richard J. Wheatley^{ab}

^a Department of Chemistry, University of Durham, Durham, UK

^b Department of Chemistry, University of Nottingham, University Park, Nottingham, UK

Online Publication Date: 10 April 1996

To cite this Article: Wheatley, Richard J. (1996) 'The solvation of sodium ions in water clusters: intermolecular potentials for Na-H₂O and H₂O-H₂O', Molecular

Physics, 87:5, 1083 - 1116

To link to this article: DOI: 10.1080/00268979600100751

URL: <http://dx.doi.org/10.1080/00268979600100751>

PLEASE SCROLL DOWN FOR ARTICLE

Full terms and conditions of use: <http://www.informaworld.com/terms-and-conditions-of-access.pdf>

This article maybe used for research, teaching and private study purposes. Any substantial or systematic reproduction, re-distribution, re-selling, loan or sub-licensing, systematic supply or distribution in any form to anyone is expressly forbidden.

The publisher does not give any warranty express or implied or make any representation that the contents will be complete or accurate or up to date. The accuracy of any instructions, formulae and drug doses should be independently verified with primary sources. The publisher shall not be liable for any loss, actions, claims, proceedings, demand or costs or damages whatsoever or howsoever caused arising directly or indirectly in connection with or arising out of the use of this material.

The solvation of sodium ions in water clusters: intermolecular potentials for $\text{Na}^+\text{-H}_2\text{O}$ and $\text{H}_2\text{O-H}_2\text{O}$

By RICHARD J. WHEATLEY†

Department of Chemistry, University of Durham, South Road, Durham DH1 3LE, UK

(Received 4 August 1995; accepted 26 October 1995)

New model potentials are constructed for $\text{Na}^+\text{-H}_2\text{O}$ and $\text{H}_2\text{O-H}_2\text{O}$, using quantum mechanical calculations of the monomer wavefunctions. One parameter in each model potential is fitted to experimental dimer properties. The resulting $\text{Na}^+\text{-H}_2\text{O}$ potential is consistent with published thermodynamic and *ab initio* data, and the $\text{H}_2\text{O-H}_2\text{O}$ potential reproduces the structure and energy of the water dimer at equilibrium, and the second virial coefficient of steam, within experimental uncertainties. The donor–acceptor interchange tunnelling pathway on the water dimer potential energy surface has a lower energy barrier than the acceptor–acceptor interchange, in agreement with recent spectroscopic studies. When a simple non-additive induction potential is included, calculated thermodynamic properties of solvated sodium ions are in agreement with experimental data. For small clusters in the gas phase, the first solvation shell of the sodium ion is predicted to contain four water molecules.

1. Introduction

The eventual aim of this work is to describe the properties of sodium ions in aqueous solution, including structure, energetics, dynamics and spectroscopy, at a microscopic level. For a study of this kind to give realistic results, it is essential that the intermolecular potentials for the ion–water and water–water interactions are known accurately, and this paper is devoted to the development of new model potentials for these two important dimers.

The properties of ionic sodium–water clusters, consisting of a few water molecules around a single ion, are used to construct and test the model potentials. Small clusters, both ionic and neutral, are formed experimentally in molecular beams, as well as naturally in the atmosphere, and recent measurements and analyses of their spectra have given detailed and valuable information on intermolecular potentials [1–4]. Neutral dimers have been studied most, but trimers are also of great interest, since they will help in developing non-additive intermolecular potentials, and larger clusters will give a greater understanding of nucleation processes and the transition from gas-phase to condensed-phase properties. A practical reason for using the properties of ionic clusters in this work, instead of aqueous solutions, is that clusters are easier to model in computer simulations than solids or liquids; for example, periodic boundary conditions and Ewald summation are not necessary.

Although ionic clusters are more difficult to form in a molecular beam than neutral clusters, some spectroscopy has been possible, including vibrational predissociation

† Present address: Department of Chemistry, University of Nottingham, University Park, Nottingham NG7 2RD, UK.

[5], photofragmentation [6–8], photoelectron spectroscopy [9] and infrared absorption [10]. The ionic clusters have included alkali metals with ethanol and propanone, aromatic molecules with rare gases, negative ions in water, and H_3O^+ in water. However, clusters of water molecules around small alkali metal ions have not yet been studied. This means that the methods used successfully to obtain potential energy surfaces for neutral species, which involve fitting a large number of parameters to high-resolution spectroscopic data, are not yet applicable to the $\text{Na}^+\text{-H}_2\text{O}$ interaction. Other experimental data provide less information. The mobilities of sodium ions in water vapour would give little more than a spherically averaged picture of the interaction, and thermodynamic information for the dimer is sensitive to essentially only the well depth at the equilibrium position. The potential energy surfaces in this work have therefore been developed in the knowledge that experimental data will provide, at most, only one or two parameters. Most of the detail of the model potentials is obtained from first principles, using quantum mechanical calculations of the properties of the interacting molecules.

There are two ways in which *ab initio* quantum mechanical calculations can be used to obtain potential energy surfaces. Using the supermolecule method, the energy of the A–B dimer is calculated by solving the electronic Schrödinger equation, and the energies of separated A and B molecules are subtracted to give the intermolecular potential. Correlated calculations with large basis sets must be used, or the results can be in error by orders of magnitude. Even the most accurate calculations disagree substantially; an example is given later in this paper for the water dimer, where the disagreement is about 20%. One of the uncertainties is caused by the choice of basis set for separated molecules A and B. If the energy of A is calculated using only the basis set of A, the resulting intermolecular potential contains basis set superposition error, which tends to make the potential well too deep. A counterpoise correction [11] is often applied by using the combined basis sets of A and B to calculate the energy of the separated molecules. This is believed to remove the basis set superposition error [12], but there remains a basis set incompleteness error, which can be of similar size to the superposition error, and is likely to make the potential well too shallow. It is almost always infeasible to use basis sets large enough to reduce the basis set incompleteness error to an acceptable level.

Since supermolecule calculations appear to be incapable, at present, of giving even one reliable potential energy value for the water dimer, they will certainly not be useful for exploring its full potential energy surface, which is six-dimensional, or twelve-dimensional if the molecules are not constrained to be rigid. Many thousands of calculations would be required to cover the surface adequately. When studying ionic solvation, in particular, it is important to have a potential energy surface for the water dimer which is reliable over a large volume of configuration space. The positions of the solvating water molecules tend to be constrained by the ion, which means that nearest-neighbour water molecules in the solvation shell generally repel one another, in contrast to bulk liquid where they attract by hydrogen bonding. The breakdown of the hydrogen-bonded water structure close to an ion will therefore depend on the details of the water potential for both attractive and repulsive geometries.

An alternative way of using *ab initio* quantum mechanical calculations, called the systematic method in the context of this work, is based on an analysis of separate physical contributions to the intermolecular potential, with some experimental information also incorporated into the final model. (The word ‘systematic’ refers to the fact that the use of *ab initio* calculations, and, in particular, the synthesis of *ab initio*

and experimental data, is performed in a systematic way, which does not vary in detail from one system to another.) Supermolecule calculations can be partitioned into components such as electrostatic, repulsion, induction and dispersion using perturbation theory [13–15], and each component can be fitted to a separate functional form. Although this straightforward partitioning of the energy is apparently still dependent on the supermolecule method, it has been shown that accurate models can be obtained for most of the components using quantum mechanical calculations on the isolated monomers only, with no dimer calculations. This reduces the computational burden from many thousands of dimer calculations to a single calculation on each monomer, and therefore enables larger basis sets to be used. Basis set superposition error is also eliminated. The accuracy of the systematic method depends principally on the accuracy with which each of the components of the energy can be modelled, as well as on the amount of high-quality experimental data that can be included. The electrostatic energy is simply the classical interaction between ground-state charge densities, and can be calculated and modelled with arbitrarily small errors. The induction and dispersion energies can both be represented by power series in inverse molecular separation, when the separation is large, and the coefficients of the power series are related in a simple manner to the molecular polarizabilities, multipoles and dispersion energy coefficients, which can be obtained either experimentally or quantum mechanically. The main difficulty arises for small separations, when the repulsion energy is important and the power series for the induction and dispersion energies are no longer valid. Modelling these short-range contributions to the intermolecular potential has been the limiting factor in the accuracy of this approach.

In this work, an overlap model is used for the repulsion component of the potential [16]. This model was applied first to neutral diatomic molecules [16, 17], but recently has been used successfully for methanol [18], hydrazine [19] and $\text{Li}^+\text{-H}_2\text{O}$ [20]. It requires only the ground-state charge densities of the monomers, so it is fully in keeping with an approach based on monomer *ab initio* calculations. As a result, it is more generally applicable than the Hartree–Fock plus damped dispersion (HFD) [21–24] and Tang–Toennies [25, 26] models for the repulsion energy, both of which rely on supermolecule calculations at the Hartree–Fock level. The exchange–Coulomb (XC) model [27–31] is closer in spirit to the overlap model, particularly in using only ground-state charge densities to calculate the repulsion energy, and it has proved successful in modelling spherical potentials between atoms, but has not yet been used widely for polyatomics.

The new potentials for $\text{Na}^+\text{-H}_2\text{O}$ and $\text{H}_2\text{O}\text{-H}_2\text{O}$, based on a systematic partitioning of the intermolecular potential and on the overlap model for the repulsion energy, are described in sections 2 and 3. Larger clusters are considered in sections 4 and 5. A non-additive potential is required for clusters of two or more molecules around an ion, and is given in section 4. In section 5, simulations of small clusters, with up to six water molecules and one ion, are described, and the structural and energetic features of the clusters are discussed and compared with experiment and with other potentials.

Atomic units are used in this paper; the atomic unit of length used is the bohr, $a_0 = 5.291\,772\,49 \times 10^{-11}$ m, and the atomic unit of energy used is the Hartree, $E_h = 4.359\,748\,2 \times 10^{-18}$ J.

2. The Na⁺-H₂O potential

The model potential has the SI (denoting Systematic potential for Ionic clusters) functional form described previously [20] for Li⁺-H₂O. The water molecule is assumed to be rigid, with the oxygen nucleus at the origin, and hydrogen nuclei at ($\pm 1.4305, 0, -1.1071$) in the molecular coordinate system. Local axes are also introduced at each nucleus. They are all parallel to the corresponding molecular axes, except for the H nucleus at (1.4305, 0, -1.1071), where the local x and y axes are reversed in direction for symmetry reasons, as shown in figure 1. The SI potential is a function of the lengths (R_0, R_1, R_2) of the vectors from the O and H nuclei to Na, and the orientations ($\Omega_0, \Omega_1, \Omega_2$) of these vectors in the local coordinate systems of the O and H nuclei. The orientation dependence is expressed using real modified spherical harmonic functions C_{l_0} and $C_{l_{mc}}$ [32].

The total potential is a sum of electrostatic, repulsion, induction and dispersion contributions, including a damping function that is designed to correct the multipolar induction and dispersion energies for the effects of charge density overlap. A scaling parameter is included in the repulsion energy, and fitted to experimental data. The functional form and parameters for each component of the potential are described below; the specific choice of parameters made in this work defines a new Na⁺-H₂O model potential which is denoted SI1.

2.1. Electrostatic energy

The electrostatic energy is the classical Coulomb interaction between the ground-state charge distributions of the ion and the water molecule. The charge distribution of water is represented using atomic multipoles, which are derived from a distributed multipole analysis [33, 34] of the water monomer wavefunction. Multipoles of higher rank than octopole are ignored, and the quadrupoles and octopoles on the hydrogen nuclei are moved to the oxygen nucleus, giving a set of atomic multipoles comprising point charges and dipoles located at all three nuclei, plus point quadrupoles and octopoles on oxygen. The electrostatic interaction of these multipoles with the charge of the ion is given by

$$E_{\text{elec}} = M_e \sum_a \sum_{lm} Q_{l_{mc}, a} C_{l_{mc}}(\Omega_a) R_a^{-(l+1)}, \quad (1)$$

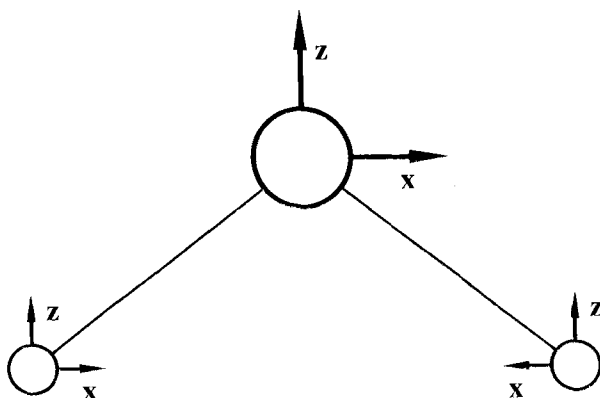
in which the subscript a denotes the nuclei of the water molecule and $Q_{l_{mc}, a}$ is a point multipole on nucleus a . The multipole moments used in this work are obtained [20] from a self-consistent field (SCF) calculation on the water molecule, and are given in table 1. The SCF wavefunction gives a dipole moment that is larger than the experimental gas phase dipole moment of the water molecule [35], so a correcting factor $M_e = 0.933$ is included in equation (1). This representation of the electrostatic energy is taken directly from the Li⁺-H₂O potential [20]. As for Li⁺-H₂O, the non-multipolar first-order Coulomb energy is assumed to be negligible.

2.2. Repulsion energy

Short range repulsion in the dimer is caused mostly by electron exchange between the monomers. It is fundamentally a dimer property, and cannot be computed directly from isolated monomer wavefunctions. A 'first-order' contribution to the exchange energy can be calculated using Heitler-London perturbation theory, but higher-order

Table 1. Parameters for the SII Na⁺-H₂O potential. All quantities are in atomic units.

Multipoles	Repulsion	Polarizabilities	Damping and scaling
$Q_{00,O} = -0.83552$	$a_{00}^0 = 48.305$	$\alpha_{00}^{11} = 9.64$	$p_1 = 1.2069$
$Q_{10,O} = 0.17094$	$a_{00}^1 = 5.886$	$\alpha_{11}^{11} = 9.81$	$p_2 = -0.09559$
$Q_{20,O} = -0.00944$	$a_{10}^0 = -1.539$	$\alpha_{-1-1}^{11} = 9.59$	$p_3 = 0.01017$
$Q_{22,O} = 0.43253$	$a_{10}^1 = -6.481$	$\alpha_{00}^{21} = -5.00$	$p_4 = 0.0026205$
$Q_{30,O} = -0.34420$	$a_{20}^0 = 4.904$	$\alpha_{20}^{21} = -2.85$	$p_5 = 1.12$
$Q_{32,O} = 0.64665$	$a_{22}^0 = 60.873$	$\alpha_{11}^{21} = -9.93$	$\chi_{00} = 4.74$
$Q_{00,H} = 0.41776$	$a_{22}^1 = -19.467$	$\alpha_{-1-1}^{21} = -4.55$	$\chi_{10} = -0.30$
$Q_{10,H} = -0.01266$	$a_{30}^0 = 6.453$	$\alpha_{00}^{22} = 42.4$	$\chi_{22} = -0.04$
$Q_{11,H} = -0.04443$	$a_{32}^0 = -13.739$	$\alpha_{11}^{22} = 51.4$	$\chi_{30} = 0.11$
	$a_{40}^0 = 1.886$	$\alpha_{-1-1}^{22} = 43.4$	$\chi_{32} = -0.22$
	$a_{40}^1 = -1.043$	$\alpha_{22}^{22} = 45.9$	$\chi_{40} = -0.03$
	$a_{42}^0 = 2.615$	$\alpha_{-2-2}^{22} = 42.8$	$\chi_{42} = 0.02$
	$B_O = 2.4113$		
	$A_H = 2.6921$	$C_6 = 8.53$	
	$B_H = 2.5$		

Figure 1. Local axis systems for the water molecule. The local y axes are at right angles to the plane of the figure, and their directions are chosen to give a right-handed axis system at each nucleus.

terms cannot be neglected, especially for strongly bound complexes. Direct *ab initio* calculation of the exchange-repulsion energy would be expensive and prone to basis set superposition error. An empirical model is therefore used [16]. The repulsion energy is assumed to be proportional to the charge density overlap integral S_ρ , which is defined by

$$S_\rho = \int \rho_A(\mathbf{r}) \rho_B(\mathbf{r}) d\mathbf{r}, \quad (2)$$

where $\rho_A(\mathbf{r})$ and $\rho_B(\mathbf{r})$ are the electronic charge densities of the unperturbed monomers.

There is one proportionality parameter K_r in this overlap model for the repulsion energy,

$$E_{\text{rep}} = K_r S_\rho. \quad (3)$$

This parameter could, in principle, be obtained from supermolecule calculations, but this would be done only as a last resort: it seems much more reasonable to fit it to experimental data, if suitable data are available. For ion-water clusters, K_r can be fitted to thermodynamic data, as described in section 2.4.

The charge densities required for the overlap model are calculated from self-consistent field (SCF) monomer wavefunctions in the current work. The basis set used for water has been described previously [20]. A 24s12p basis set is used for Na^+ , with geometric progressions of Gaussian exponents

$$\alpha_{n,s} = \alpha_{1,s} \beta_s^{n-1}, \quad n = 1-24 \quad (4)$$

$$\alpha_{n,p} = \alpha_{1,p} \beta_p^{n-1}, \quad n = 1-12 \quad (5)$$

and $\alpha_{1,s} = 0.303$ au, $\alpha_{1,p} = 0.24$ au, $\beta_s = 2.04$, $\beta_p = 2.20$. The resulting SCF energy is $-161.676948 E_h$. The charge density overlap integral S_ρ , defined in equation (2), is calculated using the GMUL program [36] at 100 dimer geometries with $3 a_0 \leq R_O \leq 5 a_0$, and fitted to an anisotropic atom-atom function

$$S_\rho = \sum_a A_a(R_a, \Omega_a) \exp(-B_a R_a) \quad (6)$$

in which the ion-oxygen anisotropy A_O has the general form

$$A_O = \sum_{lm} a_{lm}(R_O) C_{lmc}(\Omega_O). \quad (7)$$

Eight a_{lm} coefficients are used in the fit, as for $\text{Li}^+-\text{H}_2\text{O}$ [20], and the coefficients a_{00} , a_{10} , a_{22} and a_{40} are taken to be linear functions of R_O , with $a_{lm}(R_O) = a_{lm}^0 + a_{lm}^1 R_O$; the other a_{lm} coefficients are made independent of R_O . The ion-hydrogen pre-exponential factor A_H is assumed to be isotropic and constant. The resulting fitted parameters are given in table 1. The rms percentage fitting error is 1.45%, which is not reduced significantly by allowing A_H to be anisotropic.

2.3. Induction and dispersion

After the electrostatic energy, the induction and dispersion energies are the most important contributions to the long range intermolecular potential. They are written as the product of a multipole expansion up to inverse sixth power of separation, and a corrector-damping function \bar{G}^+ :

$$E_{\text{ind}} = (E_{i4} + E_{i5} + E_{i6}) \bar{G}^+[S(\Omega_O) R_O], \quad (8)$$

$$E_{\text{disp}} = -C_6 R_O^{-6} \bar{G}^+[S(\Omega_O) R_O]. \quad (9)$$

The multipolar induction energy contributions E_{i4} , E_{i5} and E_{i6} depend only on the polarizabilities $\alpha_{mm}^{i'}$ of the water molecule, and therefore are the same as for the $\text{Li}^+-\text{H}_2\text{O}$ potential:

$$E_{i4} = -\frac{1}{2}[\alpha_{00}^{11} C_{10}(\Omega_O)^2 + \alpha_{11}^{11} C_{11c}(\Omega_O)^2 + \alpha_{-1-1}^{11} C_{11s}(\Omega_O)^2]/R_O^4, \quad (10)$$

$$E_{i5} = -[\alpha_{00}^{21} C_{20}(\Omega_O) C_{10}(\Omega_O) + \alpha_{11}^{21} C_{21c}(\Omega_O) C_{11c}(\Omega_O) + \alpha_{-1-1}^{21} C_{21s}(\Omega_O) C_{11s}(\Omega_O) + \alpha_{20}^{21} C_{22c}(\Omega_O) C_{10}(\Omega_O)]/R_O^5, \quad (11)$$

$$E_{i6} = -\frac{1}{2}[\alpha_{00}^{22} C_{20}(\Omega_O)^2 + \alpha_{11}^{22} C_{21c}(\Omega_O)^2 + \alpha_{-1-1}^{22} C_{21s}(\Omega_O)^2 + \alpha_{22}^{22} C_{22c}(\Omega_O)^2 + \alpha_{-2-2}^{22} C_{22s}(\Omega_O)^2]/R_O^6. \quad (12)$$

The polarizabilities, and the dispersion energy coefficient C_6 , are given in table 1. The dispersion energy is a relatively small component (3% or less) of the total potential, so C_6 is simply assumed to be the geometric mean of the spherical dispersion energy coefficients for $\text{H}_2\text{O}-\text{H}_2\text{O}$, 45.37 au [37], and Na^+-Na^+ , 1.604 au [38].

The corrector-damping function \bar{G}^+ must be 1 at long range, where charge density

overlap is negligible and the multipole approximation is essentially exact, but at short ranges \bar{G}^+ must fall to zero at least as quickly as R^6 , as E_{ind} and E_{disp} must remain finite. Both these criteria are satisfied using the function [20, 39]

$$\bar{G}^+(x) = [1 - 8.5 \exp(-p_1 x - p_2 x^2 - p_3 x^4) + 7.5 \exp(-p_5 x)]^6, \quad (13)$$

in which the parameters p_1 – p_5 are assumed to be transferable between similar systems. Their values, taken from earlier work [39], are given in table 1. The argument x is assumed to vary as the inverse ‘size’ of the interacting species, since damping functions appropriate for larger species generally tend to 1 more slowly than for smaller species as the separation is increased. In this work, the ‘size’ (denoted χ) is allowed to vary with orientation, because the water molecule will appear larger in some directions than in others. Since the damping depends on charge overlap, χ is determined, for each orientation, by bringing in the ion until the charge density overlap S_ρ reaches 0.001 au. Using the fit to S_ρ given in section 2.2, χ is calculated for 200 different orientations Ω_0 and fitted to the function

$$\chi(\Omega_0) = \sum_{lm} \chi_{lm} C_{lm}(\Omega_0). \quad (14)$$

Eight χ_{lm} coefficients are used in the fit, but the fitted value of χ_{20} is negligible; the remaining seven are given in table 1. The agreement with the calculated $\chi(\Omega_0)$ values is closer than 0.02 a_0 for all orientations.

The scaling function $S(\Omega_0)$ in equations (8) and (9) is then defined as

$$S(\Omega_0) = S_0 / \chi(\Omega_0), \quad (15)$$

so it depends inversely on size, as required. The proportionality constant S_0 is assigned a value of 3.0 [20]. If more experimental data were available for the dimer, S_0 could be treated as an adjustable parameter.

2.4. The repulsion strength parameter

The $\text{Na}^+\text{-H}_2\text{O}$ potential contains one adjustable parameter, K_r , which scales the repulsion energy. Its value is determined by fitting to the free energy and enthalpy of complexation, which have been measured experimentally by Džidić and Kebarle [40], using mass spectrometry, to be $-73.6 \text{ kJ mol}^{-1}$ and $-100.4 \text{ kJ mol}^{-1}$, respectively. Dalleska *et al.* have estimated the $\text{Na}^+\text{-H}_2\text{O}$ bond energy using collision-induced dissociation of the dimer in xenon [41], and their result agrees very closely with Džidić and Kebarle. The uncertainties in the enthalpy and free energy are believed to be between 4 kJ mol^{-1} and 8 kJ mol^{-1} , based on similar experiments [42–44].

From the model potential, ΔG and ΔH can be predicted using thermodynamic perturbation theory [44, 45], or by direct integration of the partition function [20]: the two methods give results that agree to about 0.1 kJ mol^{-1} . It is found that K_r can be adjusted to give very good agreement with both the free energy and enthalpy. The value chosen for the SI1 $\text{Na}^+\text{-H}_2\text{O}$ potential is $K_r = 3.93 \text{ au}$, which gives $\Delta G = -73.9 \text{ kJ mol}^{-1}$ and $\Delta H = -99.9 \text{ kJ mol}^{-1}$. The resulting potential has a well depth of $38.556 \times 10^{-3} E_h$, with an equilibrium ion–oxygen distance of $4.157 a_0$, and C_{2v} symmetry. When K_r is changed by 0.1 au , the calculated free energy and enthalpy both change by about 0.5 kJ mol^{-1} , so the maximum uncertainty in K_r is about 0.8 atomic units. This corresponds to an uncertainty in well depth of $1.7 \times 10^{-3} E_h$, and an uncertainty in the equilibrium separation of $0.1 a_0$.

The well parameters predicted by the SI1 potential are in very good agreement with a number of other published calculations, including correlated *ab initio* supermolecule

calculations with reasonably large basis sets. At the MP2 level, the well depth has been estimated as $39.35 \times 10^{-3} E_h$ by Magnusson [46], and $39.52 \times 10^{-3} E_h$ by Bauschlicher *et al.* [47]. Several workers have included correlation beyond MP2: Špirko *et al.* performed MCSCF calculations around the minimum, and fitted them to obtain a well depth of $39.2 \times 10^{-3} E_h$ [48], and Bauschlicher *et al.* used CCSD(T) calculations [47] to give $39.68 \times 10^{-3} E_h$. These last calculations are probably the most accurate to have been performed on the dimer, but the monomer basis set was still smaller than the basis set used in the present work. Bauschlicher *et al.* pointed out that the basis set superposition error in their results is of order $1.5 \times 10^{-3} E_h$, and they also found a strong dependence of the calculated well depth on the basis set. The uncertainty in the *ab initio* results is therefore similar to the estimated uncertainty in the SI1 potential, and accounts easily for the discrepancy of $1 \times 10^{-3} E_h$ or so.

The equilibrium separations obtained from the *ab initio* calculations are usually about $4.21 a_0$, and therefore agree with the SI1 potential to within its estimated uncertainty. It is possible that the SI1 bondlength is too short, since it is slightly shorter than all the *ab initio* results. Microwave spectroscopy on the dimer would resolve this difference, and would also provide much more reliable data for fitting the parameter(s) in the SI functional form.

It is interesting that SCF supermolecule calculations give a well depth of $38.72 \times 10^{-3} E_h$ [49], which is in fortuitously good agreement with the correlated calculations and the SI1 potential. This arises from a cancellation of errors. The SCF dipole moment of water is too large, so the electrostatic energy is overestimated, but the polarizability of water is too small, and the $\text{Na}^+-\text{H}_2\text{O}$ dispersion energy coefficient is zero in the SCF approximation, which means that the induction and dispersion energies are both underestimated. In this particular case, the cancellation is almost exact.

The well depth of the SI1 potential also agrees with the POL1 potential developed by Caldwell *et al.* [50] to within $0.5 \times 10^{-3} E_h$. This is to be expected, since both potentials are fitted to the experimental enthalpy of complexation, although the fit to the SI1 potential also includes the free energy. However, for $\text{Li}^+-\text{H}_2\text{O}$ a fit to the free energy [20] gave quite different results from other literature potentials, which had been fitted to the enthalpy. This difference can be explained by the experimental results. For $\text{Na}^+-\text{H}_2\text{O}$ the enthalpy of complexation was measured directly by Džidić and Kebarle [40], and it is therefore expected to be more reliable than for $\text{Li}^+-\text{H}_2\text{O}$, where the enthalpy and free energy had to be extrapolated from larger clusters. One indication of the greater reliability of the results for $\text{Na}^+-\text{H}_2\text{O}$ is that the SI1 model potential agrees well with both the enthalpy and free energy, which was not the case for $\text{Li}^+-\text{H}_2\text{O}$.

Cuts through the three-dimensional SI1 potential energy surface as shown in figure 2 for in-plane, 45° and 90° out-of-plane geometries. As the ion is moved away from its equilibrium position, while remaining the same distance from the oxygen nucleus, the upward curvature of the potential is much greater when the ion remains in the plane of the water molecule than when it moves out of the plane towards the 'lone pair' positions. This difference is due to electrostatic effects, mainly the repulsion of the ion by the positively charged hydrogen nuclei. The effect becomes more pronounced as the geometry is distorted further. In out-of-plane geometries the ion can move more than 90° round the molecule towards the hydrogen nuclei before the potential well disappears, but in the molecular plane the repulsion between the ion and the hydrogen nuclei has a greater effect. The shape of the repulsive wall in the plane is a distorted triangle, reflecting approximately the shape of the water molecule.

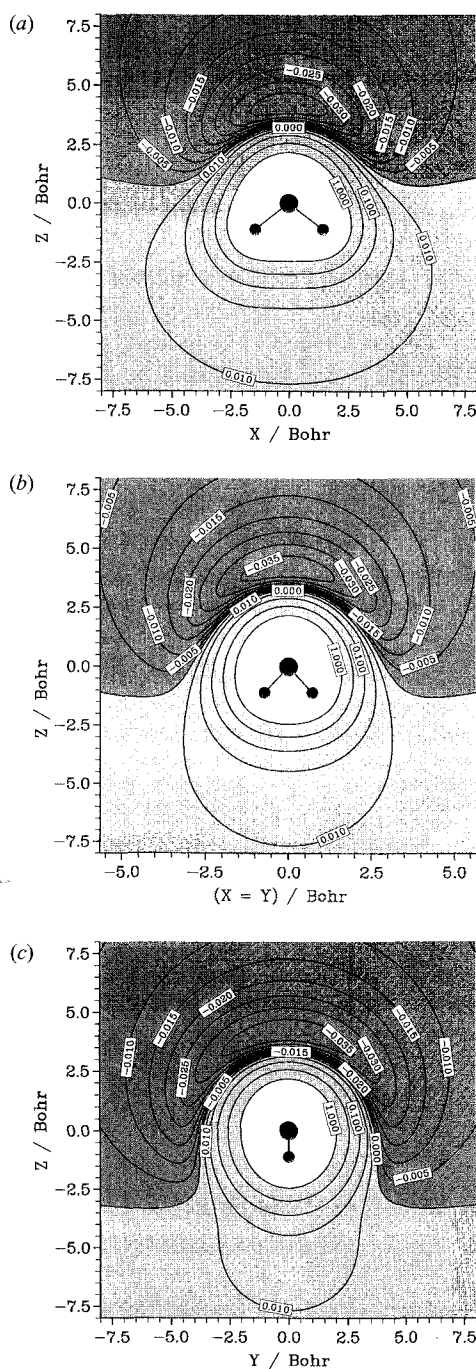


Figure 2. Contours of the SH1 $\text{Na}^+\text{-H}_2\text{O}$ potential energy surface. Contour labels indicate potential energies as E/E_h , and are drawn at $E = -0.035, -0.005, 0.0, 10^{-2}, 10^{-1.5}, 10^{-1}, 10^{-0.5}$ and $10^0 E_h$. In (a) the ion is in the plane of the water molecule; in (b) it is in a plane that includes the water C_2 axis and makes an angle of 45° with the molecular plane, and in (c) it is in a plane bisecting the H nuclei. The positions of the O and H nuclei are projected onto the plane of the figure and shown to scale.

3. The H₂O–H₂O potential

A new model potential for water has been developed, using the systematic potential method. It is designed to be used with the S11 ion–water potentials, given in section 2 and in [20], in simulations of ion solvation, although it would probably be reasonably reliable as a pure water potential. It can be used to describe systems ranging from dimers to bulk liquid, since the pair contributions and many-body contributions are considered separately.

The development of a model potential for water is also an interesting test of the systematic potential method. Many more potentials have been published for the water dimer than for other interactions described previously using the systematic method, so more detailed comparisons can be made. The systematic method is well suited to calculating the water dimer potential. Monomer wavefunctions are an essential ingredient of the method, and water molecules are small enough to allow accurate wavefunctions to be calculated. In addition, the contributions to the potential that are described more accurately using monomer wavefunctions, such as the electrostatic energy, are also the most important in determining the main anisotropic features of the water dimer potential.

The systematic potential for water (denoted SW) is partitioned into electrostatic (first-order Coulomb), dispersion, induction and repulsion contributions,

$$E = E_C^{(1)} + E_{\text{disp}} + E_{\text{ind}} + E_{\text{rep}}. \quad (16)$$

No explicit charge-transfer or hydrogen-bonding contributions are included. There is a reasonable amount of evidence to suggest that the phenomenon of hydrogen bonding is largely electrostatic in origin [51–53], and it is therefore already included in the first-order Coulomb energy, with no need to invoke a separate physical effect. Charge transfer, on the other hand, can be a significant part of the potential. The four components on the RHS of equation (16) can be considered to arise from the following contributions to the dimer wavefunction, respectively: the unperturbed monomer wavefunctions (A, B); the use of virtual orbitals of both molecules simultaneously (A → A*, B → B*); the use of virtual orbitals of each molecule separately (A → A* and B → B*); and exchange of electrons between the occupied orbitals of the molecules (A → B, B → A). The charge-transfer energy would describe the excitation of electrons from occupied orbitals on one molecule to virtual orbitals on the other (A → B* and B → A*), which is apparently a separate effect. However, in the limit of an infinite basis set, there is no distinction between the virtual orbitals of the molecules, and the charge transfer simply becomes part of the induction energy. Any definition of the charge-transfer energy will therefore depend heavily on the basis set. The usual definition of Morokuma [13, 14] also includes a significant amount of basis set superposition error. Two other definitions have been proposed, by Glendening and Streitwieser [54] and by Stone [55]. These are claimed to be free of basis set superposition error. Unfortunately, for the water dimer, Stone's definition gives a charge transfer energy that is much smaller than the Morokuma value, but Glendening and Streitwieser's definition gives a much larger result. The disagreement is more than an order of magnitude. Furthermore, to implement either definition requires *ab initio* calculations that are almost as expensive as full supermolecule calculations, and these would have to be performed over the entire six-dimensional potential energy surface. A simple way to proceed is suggested by Stone's calculations [55], which show that (using his definition) the charge-transfer energy is negative, and at low-energy points on the dimer surface

it is reasonably proportional to the repulsion energy, which is always positive. The charge-transfer energy is therefore included implicitly in the potential energy surface developed in the present work, using an empirical parameter to scale the repulsion energy, which is in any case an inherent part of the systematic potential method. Using large-scale *ab initio* calculations to improve this representation of the charge-transfer energy seems premature at the present time, given the uncertainties in the model for the repulsion energy, which is much larger.

Functional forms for each of the components in equation (16) are described in sections 3.1–3.4. They are obtained from analysis of monomer wavefunctions, rather than supermolecule calculations, as discussed in section 1. Only one adjustable parameter is included in the potential, and is fitted to experimental second virial coefficient data. The form of the final SW potential is described, and compared with published potentials, in sections 3.5 and 3.6.

3.1. Electrostatic energy

The electrostatic (first-order Coulomb) interaction energy $E_C^{(1)}$ is defined by

$$E_C^{(1)} = \iint \rho_A(\mathbf{r}_1) \rho_B(\mathbf{r}_2) r_{12}^{-1} d\mathbf{r}_1 d\mathbf{r}_2 - \sum_{a \in A} Z_a \int \rho_B(\mathbf{r}_2) r_{a2}^{-1} d\mathbf{r}_2 \quad (17)$$

$$- \sum_{b \in B} Z_b \int \rho_A(\mathbf{r}_1) r_{1b}^{-1} d\mathbf{r}_1 + \sum_{a \in A} \sum_{b \in B} Z_a Z_b r_{ab}^{-1},$$

where ρ_A and ρ_B are the electron densities of molecules A and B, and Z_a is the atomic number of nucleus a of molecule A. The first-order Coulomb interaction energy can be partitioned into the familiar multipolar contribution $E_m^{(1)}$ and the penetration (non-multipolar first-order Coulomb) energy $E_p^{(1)}$.

The multipolar first-order Coulomb interaction energy between two water molecules is represented as a sum of interactions between the atomic multipoles Q_{lm} given in table 1.

$$E_m^{(1)} = \sum_{ab} \sum_{lm, l'm'} Q_{lm, a} Q_{l'm', b} T_{lm, l'm'}(R_{ab}, \Omega_{ab}), \quad (18)$$

where $T_{lm, l'm'}$ is a function of the internuclear separation R_{ab} , and of the orientation Ω_{ab} of the local coordinate systems of the nuclei a and b (defined in figure 1) relative to the internuclear vector. The T functions have been tabulated for $l+l' \leq 4$ [32], and they can also be derived for higher multipole rank [56]. In this work, multipolar interactions with $l+l' > 4$ are ignored. The inclusion of these quadrupole–octopole and octopole–octopole terms would add greatly to the complexity of the potential, and the accuracy gained would be considerably less than 1% in the region where the multipole approximation is reasonable, that is, from the potential well outwards.

The penetration energy $E_p^{(1)}$ is defined as the difference $E_C^{(1)} - E_m^{(1)}$. To assess the importance of penetration for the water dimer in its equilibrium geometry, the first-order Coulomb interaction energy is calculated from the SCF monomer wavefunction used previously for the water molecule [20], using the GMUL program [36], and is found to be $-15 \times 10^{-3} E_h$. The multipolar electrostatic energy is calculated, using the same wavefunction, to be $E_m^{(1)} = -12 \times 10^{-3} E_h$. The penetration energy is therefore $E_p^{(1)} = -3 \times 10^{-3} E_h$, which is about 40% of the binding energy. This result is believed

to be fairly reliable, and shows that the penetration energy is a major component of the potential; for example, it is over twice the size of the charge transfer energy calculated by Stone [55]. The large value of the penetration energy for the water dimer is a result of the short O–H hydrogen-bonding distance, which allows the proton to ‘penetrate’ inside the charge density of the oxygen atom. An explicit representation of the penetration energy is therefore believed to be important in describing this interaction.

Using the GMUL program, and the same wavefunction for the water molecule, the first-order Coulomb interaction energy $E_C^{(1)}$ is calculated at 100 different dimer geometries, with O–O distances between $4 a_0$ and $8 a_0$. The multipolar electrostatic energy is calculated at the same points, using equation (18), and subtracted to give the penetration energy $E_p^{(1)}$. This is found to be negative for all the geometries considered, whereas both positive and negative values of the multipolar and non-multipolar first-order Coulomb interaction energy occur. The penetration energy is generally expected to be negative for neutral molecules at physically reasonable geometries, because the multipole approximation takes no account of charge density overlap and therefore overestimates the positive electron–electron repulsion. However, the penetration energy would certainly become positive at small internuclear separations [31].

The penetration energy is fitted to an anisotropic atom–atom function:

$$E_p^{(1)} = \sum_{ab} \exp(-\alpha_{ab} R_{ab}) \sum_{lm,l'm'} A_{lm,l'm'}^{ab} S_{l,l',l''}^{m,m'}(\Omega_{ab}), \quad (19)$$

where a and b are summed over the nuclei on molecules A and B, and S is a function of orientation, defined by [57]

$$S_{l,l',l''}^{m,m'} = i^{l'-l-l''} \sum_{k,k',k''} \begin{pmatrix} l & l' & l'' \\ k & k' & k'' \end{pmatrix} D_{km}^l(\omega_a)^* D_{k'm'}^{l'}(\omega_b)^* D_{k''0}^{l''}(\omega)^*. \quad (20)$$

In this equation, ω_a , ω_b and ω are the orientations of the local axes of nuclei a and b , and of the vector from a to b , relative to a space-fixed axis system. The D functions are Wigner rotation matrices, and the coefficient in large parentheses is a Wigner 3-j symbol [58]. The S functions are complex, but real components can be defined using

$$S_{l,l',l''}^{m,c,0} = 2^{-1/2} [(-1)^m S_{l,l',l''}^{m,0} + S_{l,l',l''}^{-m,0}] \quad (21)$$

and similarly for $S_{l,l',l''}^{0,m,c}$. These real functions are used in the current work for $m, m' \neq 0, 0$, but for $m, m' = 0, 0$ the definition in equation (20) is used. No S functions are used in the current work with both m and m' non-zero.

The coefficients $A_{lm,l'm'}^{ab}$ and exponents α_{ab} , obtained from a fractional least-squares fit to the penetration energy, are shown in table 2. The fitted exponents are somewhat counter-intuitive, since α_{OH} is smaller than the other two. This may be related to the fact that the penetration energy proved to be difficult to fit. Even with the 17 parameters shown, the rms percentage fitting error is 8.3%, which would correspond to a 3% error in the binding energy. The error is not reduced significantly by allowing the hydrogen nuclei to be anisotropic.

The first-order Coulomb interaction energy for the water dimer is given by the sum of the multipolar electrostatic energy (equation (18)) and the penetration energy (equation (19)), corrected for the SCF dipole moment, as in section 2.1, by multiplying by the factor M_e^2 :

$$E_C^{(1)}(\text{model}) = M_e^2 (E_m^{(1)} + E_p^{(1)}). \quad (22)$$

This expression for $E_C^{(1)}(\text{model})$ is that used in the SW model potential. As before,

Table 2. Parameters of the SW $\text{H}_2\text{O}-\text{H}_2\text{O}$ potential, in atomic units, as defined in equations (19), (25) and (30). Parameters with $m \neq 0$ multiply the real S functions defined in equation (21), and are given in the table with a factor of $2^{1/2}$, which cancels the factor $2^{-1/2}$ in equation (21). All parameters are unaffected by interchanging (a, l, m) and (b, l', m') .

Penetration	Dispersion	Repulsion
$a, b = \text{O}, \text{O}$	$a, b = \text{O}, \text{O}$	$a, b = \text{O}, \text{O}$
$A_{00,00} = -96.426$	$C_{6,000}^{00} = 64.43$	$B_{00,00} = 36.439$
$A_{10,00} = -27.765$	$C_{6,202}^{00} = 3.96$	$B_{10,00} = 14.964$
$A_{20,00} = -21.737$	$C_{6,202}^{20} = 6.98\sqrt{2}$	$B_{20,00} = 4.164$
$A_{22,00} = 33.222\sqrt{2}$	$C_{6,112}^{00} = -1.21$	$B_{22,00} = -10.941\sqrt{2}$
$A_{10,10} = 36.890$	$C_{6,404}^{00} = -3.65$	$B_{10,10} = -0.460$
$A_{30,00} = 12.083$	$C_{6,404}^{20} = 2.06\sqrt{2}$	$B_{30,00} = -3.688$
$A_{32,00} = -50.027\sqrt{2}$	$C_{7,101}^{00} = 274.4$	$B_{32,00} = 11.131\sqrt{2}$
$A_{20,10} = 14.609$	$C_{7,303}^{00} = -60.6$	$B_{20,10} = -2.703$
$A_{22,10} = -26.648\sqrt{2}$	$C_{7,303}^{20} = 77.9\sqrt{2}$	$B_{22,10} = 4.269\sqrt{2}$
$\alpha = 2.08$	$C_{7,211}^{20} = -17.1\sqrt{2}$	$\beta = 2.05$
	$C_{8,000}^{00} = 1511$	
$a, b = \text{O}, \text{H}$	$a, b = \text{O}, \text{H}$	$a, b = \text{O}, \text{H}$
$A_{00,00} = -1.837$	$C_{6,000}^{00} = -5.39$	$B_{00,00} = 1.948$
$A_{10,00} = -1.829$	$C_{7,101}^{00} = 17.1$	$B_{10,00} = 0.660$
$A_{20,00} = -0.469$	$C_{8,000}^{00} = 134$	$B_{20,00} = 0.397$
$A_{22,00} = -0.141\sqrt{2}$		$B_{22,00} = -0.718\sqrt{2}$
$\alpha = 1.88$		$\beta = 2.10$
$a, b = \text{H}, \text{H}$		$a, b = \text{H}, \text{H}$
$A_{00,00} = 0.310$		$B_{00,00} = 0.091$
$\alpha = 2.10$		$\beta = 2.07$

$M_e = 0.933$. It seems reasonable to scale the penetration energy as well as the multipolar Coulomb energy, since both arise from integrals over the charge densities, but further *ab initio* calculations are required to check this.

3.2. Dispersion energy

The dispersion energy of interaction between water molecules can be written as a damped multipole series:

$$E_{\text{disp}}(R, \Omega) = \left[\sum_{n=6}^{10} C_n(\Omega) R^{-n} \right] G(R, \Omega), \quad (23)$$

where R and Ω are the intermolecular separation and relative orientation, and the C_n are dispersion energy coefficients. The corrector-damping function G is intended to correct for the neglect of higher powers of R^{-1} , and to remove the singularity in the multipole series at $R = 0$ by accounting for charge overlap (damping) effects.

The dispersion energy coefficients can be obtained from monomer calculations of the ground-state wavefunctions, pseudostates and pseudo-excitation energies [59–61]. Correlated *ab initio* methods, and large basis sets, are required to give acceptably accurate coefficients, so the calculations are quite expensive. The best values in the literature are those calculated by Wormer and Hettema [62], who give dispersion energy coefficients $C_{n;l,l',m,m'}^{m,m'}$ for $n \leq 10$ in the expansion

$$C_n(\Omega) = \sum_{l,l',m,m'} C_{n;l,l',l',m,m'}^{m,m'} S_{l,l',l',m,m'}^{m,m'}(\Omega). \quad (24)$$

In their results, R and Ω refer to the separation and orientations of the molecular centres of mass, and they use expansion functions that differ slightly from the S functions defined in section 3.1. They tabulate 39 anisotropic dispersion energy coefficients that are not related by symmetry, and inclusion of symmetry-related coefficients increases this number by a factor of four or more.

In the current work, the number of different dispersion energy coefficients is reduced by fitting the multipolar dispersion energy calculated by Wormer and Hettema to an atom-atom function:

$$E_{\text{mult, disp}} = - \sum_{ab} \sum_n \sum_{l, l', l'', m, m'} C_{ab, n; l, l', l'', m, m'}^{m, m'} S_{l, l', l''}^{m, m'}(\Omega_{ab}) R_{ab}^{-n}. \quad (25)$$

The atom-atom dispersion energy coefficients $C_{ab, n; l, l', l'', m, m'}^{m, m'}$ in this equation are fitted at 200 different geometries with O-O separations between $6 a_0$ and $12 a_0$. An rms percentage deviation of less than 1% is obtained with 14 different coefficients, which are shown in table 2. This representation is cheaper to use than equation (24), because there are fewer terms in the sum, and because the angular momentum ranks (l, l', l'') are generally smaller in the current work. The isotropic C_6 dispersion energy coefficient from the fit, $C_6 = 42.87$ au, is 5.5% smaller than the accurate value given in section 2. This difference is surprisingly large, but not particularly serious, since the total dispersion energy is less than one quarter of the total interaction energy at the equilibrium geometry. Discrepancies in the fitted C_6 must be corrected for partly by the higher fitted coefficients, in the range of separations used for fitting.

The multipolar dispersion energy is then multiplied by a corrector-damping function G . In this work, the simple XC-1 damping function [27] is used,

$$G(R, \Omega) = \exp[-0.4(1.28R^*/R_{00} - 1)^2], \quad R_{00} < 1.28R^*, \\ = 1, \quad R_{00} > 1.28R^*. \quad (26)$$

This functional form is not completely suitable for the water dimer: for example, it does not depend on the relative orientations of the water molecules. Although it is possible to calculate damping functions using *ab initio* methods, such calculations are currently feasible only for small atoms and linear molecules.

The parameter R^* , which appears in equation (26), is the equilibrium van der Waals separation, $7.82 a_0$, for triplet H-H [27], and for other van der Waals dimers it is reasonable to assume that R^* will increase with the size of the molecules forming the dimer. For the water dimer R^* is chosen to be $8.86 a_0$, which is 1.133 times more than for H-H, because the square root of the ratio of isotropic dispersion energy coefficients $(C_8/C_6)^{1/2}$, which also reflects the size of the molecules, is 1.133 times more for the water dimer than for the H dimer. This use of dispersion energy coefficients to scale the length parameter in damping functions is justified by previous work [30, 63, 64].

3.3. Induction energy

The induction energy is also written as a damped multipole series:

$$E_{\text{ind}} = -\frac{1}{2} \sum_A \sum_{lm, l'm'} \alpha_{mm'}^{l'l'} F_{lm}^A F_{l'm'}^A \quad (27)$$

where F_{lm}^A is a component of the electric field at molecule A due to the other molecule B, and is calculated using

$$F_{lm}^A = M_e \sum_{b, l', m'} Q_{l'm', b} T_{lm, l'm'}(R_{Ab}, \Omega_{Ab}) G_{\text{ind}}(R_{AB}, \Omega_{AB}). \quad (28)$$

In these equations, α is a multipole polarizability of the water molecule, centred at the oxygen nucleus, M_e corrects for the SCF dipole moment, Q is a distributed multipole, and T is an interaction tensor. These quantities are defined in sections 2.1, 2.3 and 3.1. The maximum value of $l+l''$ in equation (28) is restricted to 2, which simplifies the model potential by removing a number of small contributions with complicated functional forms.

The function G_{ind} , which is included to account for the effect of charge density overlap on the electric field at short range, behaves as the square root of an induction energy damping function, since the induction energy calculated from equation (27) includes the square of G_{ind} . Since an appropriate induction energy damping function is not known, the function G_{ind} is replaced by the square root of the *dispersion* energy damping function G , which is defined in equation (26). A related approximation has been made by Millot and Stone [65], who also pointed out that the induction energy damping function is not a particularly important part of the potential.

3.4. Repulsion energy

The repulsion energy is estimated from the charge density overlap integral S_ρ , using a single proportionality parameter K_w ,

$$E_{\text{rep}} = K_w S_\rho. \quad (29)$$

The charge density overlap integral S_ρ is defined by equation (2). It is calculated for the water dimer for the same geometries as the penetration energy, and the results are fitted to an analogous functional form:

$$S_\rho = \sum_{ab} \exp(-\beta_{ab} R_{ab}) \sum_{lm, l'm'} B_{lm, l'm'}^{ab} S_{l, l', l+l'}^{m, m'}(\Omega_{ab}). \quad (30)$$

The best-fit parameters are given in table 2. The rms percentage fitting error is 3.9%, which is smaller than the error in the fit to the penetration energy.

The parameter K_w is fitted to experimental second virial coefficient data [66]. The second virial coefficient of water can be calculated, neglecting quantum corrections, from the integral

$$B(T) = \frac{N_A}{48\pi^2} \int \cdots \int [1 - \exp(-E/kT)] dr^3 d\cos\theta d\phi d\alpha d\cos\beta d\gamma, \quad (31)$$

where E is the intermolecular potential energy between one molecule at the origin, and a second molecule translated by (r, θ, ϕ) in spherical polar coordinates, and rotated by the Euler angles (α, β, γ) , relative to the first. Since quantum corrections will be most important at low temperatures, the high temperature experimental values are weighted most in the fit.

Two methods are used to evaluate this integral. Both depend on dividing the coordinate r into slices, which are chosen to be 0–4, 4–5.5, 5.5–7, 7–10, 10–20, 20–50 and 50–300 a_0 . The integral 0–4 a_0 is performed analytically, replacing E by ∞ . This approximation is justified, since changing the limit from 4 a_0 to 3.5 a_0 has no effect on the final result. The other coordinates are not subdivided.

The first method used to evaluate the integral over each slice (except the first) is a straightforward Monte Carlo procedure. Random points are selected in the six-dimensional space, and the value of the integrand is averaged over all the random points chosen. When 40000 points are used in each slice, the uncertainty in the result is estimated to be less than 2%.

The second method uses importance sampling and the Metropolis algorithm. For each slice, the integral

$$F(T) = \frac{N_A}{48\pi^2} \int \cdots \int \exp(-E/kT) dr^3 d \cos \theta d\phi d\alpha d \cos \beta d\gamma \quad (32)$$

is well-defined, even though it would be infinite for an infinite range of r . Although $F(T)$ cannot be evaluated directly using importance sampling, it can be differentiated to give

$$F^{-1} \frac{dF}{d(1/kT)} = \frac{d \ln F}{d(1/kT)} = \frac{-\int \cdots \int \exp(-E/kT) dr^3 \cdots d\gamma}{\int \cdots \int \exp(-E/kT) dr^3 \cdots d\gamma} \quad (33)$$

This quantity equals $-\langle E \rangle$, i.e. minus the average energy value calculated from a Monte Carlo simulation with Metropolis importance sampling. Integrating equation (33), it follows that

$$F(T) = F(\infty) \exp \left[- \int_0^{1/kT} \langle E \rangle d(1/kT) \right] \quad (34)$$

and putting $1/kT = 0$ in equation (32) gives $F(\infty) = 2\pi N_A (r_1^3 - r_0^3)/3$, where r_0^3 and r_1^3 are the bounds on the integral over r^3 . This means that it is possible to calculate the contribution to $B(T)$ from each slice, provided that $\langle E \rangle$ is known as a function of T from the required temperature up to $T = \infty$. Then $F(T)$ can be calculated from equation (34), and the contribution to $B(T)$ is $2\pi N_A (r_1^3 - r_0^3)/3 - F(T)$ for the slice from r_0^3 to r_1^3 . This procedure is based on the thermodynamic perturbation method of evaluating free energies [44].

In practice $\langle E \rangle$ is calculated by Monte Carlo simulation for $1/kT = 0, 100, 200, \dots, 900$ atomic units, then fitted to a rational function of $\beta = 1/kT$,

$$\langle E \rangle = - \frac{a_0 + a_1\beta + a_2\beta^2}{1 + b_1\beta + b_2\beta^2} \quad (35)$$

and integrated using Simpson's rule. To obtain an accuracy of 2%, it is found that up to 20000 evaluations of the potential are required for each value of $1/kT$ in each slice. About nine values of $1/kT$ are required to give second virial coefficients down to $T = 400$ K. The agreement with the straightforward Monte Carlo method is then within the estimated error of 2%.

The first (straightforward) Monte Carlo method is more efficient, since all the energy calculations can be reused at different temperatures, whereas in the importance sampling procedure a separate simulation is required at each temperature. The first Monte Carlo method is therefore used, with 400000 points in each slice. The fitted repulsion energy scaling parameter is $K_w = 6.08$ au, giving the calculated second virial coefficients shown in table 3. A change in K_w of 0.1 au changes B by about $3 \text{ cm}^3 \text{ mol}^{-1}$ at 673 K, so the value of K_w is determined by the second virial coefficient data to within about 0.05. The agreement with experiment at temperatures of 473 K and above is excellent, but at 423 K the calculated second virial coefficient is not as negative as the experimental value of Kell *et al.* [66]. However, after the current work was completed, the recent results of Eubank *et al.* [67] were discovered. These results apparently have been largely overlooked in the literature. Eubank *et al.* show that earlier measurements of second virial coefficients have been affected seriously by adsorption at low temperature, and give corrected second virial coefficients for water,

Table 3. Experimental and calculated second virial coefficients for the water dimer. Experimental second virial coefficients B_{exp} are taken from the fitted function of Kell *et al.* [66] between 423 K and 673 K, results in parentheses come from the more recent work of Eubank *et al.* [67], and from 773 K to 1173 K the results quoted by Kozack and Jordan [68] are used.

T/K	$-B_{\text{exp}}/\text{cm}^3 \text{ mol}^{-1}$	$-B_{\text{calc}}/\text{cm}^3 \text{ mol}^{-1}$
423	338 (288 ± 10)	298
473	213 (203 ± 2)	207
523	153	153
572	117	117
623	92	92.5
673	73.5	74.5
773	50.4	50.5
873	35.2	35.3
973	24.6	25.0
1073	17.0	17.7
1173	11.6	12.2

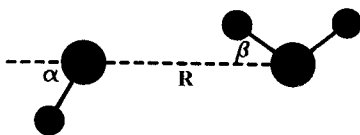


Figure 3. Structural parameters for the water dimer with C_2 symmetry, which includes the equilibrium geometry. In the acceptor molecule, the hydrogen nuclei are placed symmetrically above and below the plane of the figure. The angle α is measured between the O–O line (dashes) and the water C_2 axis.

which are shown in table 3. The new results are in excellent agreement with the results obtained from the SW potential. The high temperature results quoted by Kozack and Jordan [68] also agree with the predictions of the SW potential, to within experimental error.

The fitted parameter, $K_w = 6.08$ au, can be compared with analogous repulsion energy scaling parameters $K_r = 3.93$ for $\text{Na}^+\text{-H}_2\text{O}$, given previously in this paper, and 10.95 for $\text{Li}^+\text{-H}_2\text{O}$, obtained in earlier work [20]. This parameter clearly is not transferable between different systems, but on the other hand it changes by a factor of less than three between the three dimers.

3.5. Equilibrium structure and energy of the water dimer

It is now generally accepted that the lowest-energy structure of the water dimer is singly hydrogen bonded, with C_s symmetry. The hydrogen donor molecule lies in the symmetry plane, while the hydrogen acceptor is at right angles to the plane. If the water molecules are rigid, there are three structural parameters describing the equilibrium geometry (see figure 3): the O–O distance R , the angle β , which describes the nonlinearity of the hydrogen bond, and the angle α between the acceptor C_2 axis and the O–O direction.

Since the potential energy surface is quite flat and anharmonic around the

minimum, experiments have not, as yet, provided accurate values for any of these three parameters, or the dissociation energy ΔE from the bottom of the potential well. The values most often quoted [69, 70] have rather large uncertainties: $\alpha = 58^\circ \pm 6^\circ$, $\beta = -1^\circ \pm 6^\circ$, $\Delta E = 22.6 \pm 2.9 \text{ kJ mol}^{-1}$, and $R_0 = 2.98 \text{ \AA}$. Here R_0 is the average O–O distance in the ground vibrational state of the dimer. Its experimental value is reliable, but since it includes anharmonic effects it is likely to be larger than R . The SW potential developed in this work has the correct symmetry in the equilibrium geometry, and structural parameters in agreement with the experimental error bounds: $\alpha = 61.6^\circ$, $\beta = 5.8^\circ$, $\Delta E = 19.8 \text{ kJ mol}^{-1}$, and $R = 2.924 \text{ \AA}$.

The predicted equilibrium geometry can be compared more directly with the results of *ab initio* calculations on the water dimer. Unfortunately, *ab initio* studies have produced results that differ from each other by at least as much as the experimental uncertainties. Smith *et al.* [71] have optimized the geometry at the MP2 level, with two fairly small basis sets, obtaining $R = 2.908 \text{ \AA}$ in both cases. They calculated ΔE to be 22.7 kJ mol^{-1} (MP2), 22.0 kJ mol^{-1} (MP3) and 22.6 kJ mol^{-1} (MP4) for this geometry, but the basis set superposition error (BSSE) was more than 3.5 kJ mol^{-1} in each case. Rybak *et al.* [72] performed SAPT and MBPT4 calculations on the dimer for a few geometries; the MBPT results gave R between 2.95 and 3.00 \AA , with $\Delta E \approx 18.8 \text{ kJ mol}^{-1}$, but the SAPT calculations gave a considerably shorter and stronger bond. More recently, Feller [73] has investigated the effect of a systematic series of basis sets on the dimer energy, but using only one geometry with $R = 2.911 \text{ \AA}$. He estimated the basis set limit of ΔE to be about 21 kJ mol^{-1} , but even the largest basis set gave a BSSE in excess of 2 kJ mol^{-1} . Van Duijneveldt-Van de Rijdt and Van Duijneveldt [74] used the full counterpoise correction, at the MP2 level, in an attempt to remove the BSSE, and their largest basis set gave $\Delta E = 19.7 \text{ kJ mol}^{-1}$, with $R = 2.949 \text{ \AA}$. Saebø *et al.* [75] used a local correlation method to remove BSSE, and their most accurate result, at MP4(SDQ) level with a fairly large basis set, was $\Delta E = 19.3 \text{ kJ mol}^{-1}$. Their calculations were performed at a single point with $R = 2.97 \text{ \AA}$, and they estimate that more accurate calculations could alter the energy by 2 kJ mol^{-1} . Chakravorty and Davidson [76] also performed MP4(SDQ) calculations, with a large basis set, but with fairly large R values of 2.98 – 3.00 \AA . They obtained $\Delta E = 18$ and 19 kJ mol^{-1} , with and without the counterpoise correction, respectively. The only definite conclusion to emerge from these studies is that the experimental value of ΔE is unlikely to be too small, and may well be too large by about its quoted uncertainty. This is in agreement with the prediction of the SW potential.

A large number of model potentials have also been published for water, although many of these have been fitted to the properties of liquid and/or solid water, and do not reproduce satisfactorily the structure of the dimer. For example, the POL1 model of Dang [77] gives an O–O distance of $R = 2.82 \text{ \AA}$, which is too short, and a well depth of 23 kJ mol^{-1} , which is (probably) too deep. The effective potential of Wallqvist and Berne [78] gives a shallow minimum, $\Delta E = 14.7 \text{ kJ mol}^{-1}$, and a small acceptor angle, $\alpha = 19^\circ$.

Recent model potentials which have been designed specifically for the water dimer include the ASP potential of Millot and Stone [65], which is constructed in a similar manner to the current SW potential as a sum of Coulomb, repulsion, induction and dispersion components. One difference is that the ASP potential has no fitted parameters; the repulsion energy is calculated from the difference between the Heitler–London first-order interaction energy and the multipolar electrostatic energy. The penetration energy is therefore included in the repulsion energy. The equilibrium

geometry of the ASP potential is similar to the SW potential, except that the O–O distance is $R = 2.98 \text{ \AA}$ for the ASP. This is probably too long, whereas the SW distance may be too short. The dissociation energy $E = 19.6 \text{ kJ mol}^{-1}$ for the ASP potential is close to the SW value, and the second virial coefficients are predicted almost as well by the ASP potential as by the SW potential.

A simpler model, consisting of four point charges, a Lennard-Jones centre and a point polarizability, has been proposed recently by Kozack and Jordan [68]. The potential was fitted to second virial coefficient data, and the agreement is very good; the dimer structure is also predicted correctly. The dissociation energy is 21.5 kJ mol^{-1} , the donor and acceptor angles are in good agreement with experiment, and the equilibrium separation is $R = 2.98 \text{ \AA}$. The Kozack and Jordan model was also used in liquid simulations, but the results were not encouraging.

Another model potential, which is similar to the SW model in several ways, has been published by Åstrand *et al.* [79]. The oxygen and hydrogen atoms are assigned charges, dipoles and point polarizabilities, and a London dispersion energy is added, together with a repulsion energy based on the square of the overlap integral between the monomer wavefunctions. The resulting potential has an equilibrium O–O separation of 2.90 \AA , with a dissociation energy of 20.2 kJ mol^{-1} , and $\alpha = 65^\circ$, $\beta = 3.4^\circ$. It is interesting to note that the electrostatic energy of this model is too large, since Hartree–Fock multipole moments are used, and the London C_6 dispersion energy coefficient is too small (30.2 au), but these effects almost cancel to give a reasonable dimer energy at the minimum. Specifically, the Åstrand electrostatic energy, $-28.6 \text{ kJ mol}^{-1}$, is about 4 kJ mol^{-1} more negative than the SW multipolar electrostatic energy, and the Åstrand dispersion energy, -4.6 kJ mol^{-1} , is about 4.5 kJ mol^{-1} less negative than the SW dispersion energy.

A somewhat different approach has been adopted by Franken and Dykstra [80], who used diffusion quantum Monte Carlo simulations to fit the Lennard-Jones parameters in a model potential to experimental rotational constants. Their resulting model potential has an equilibrium O–O distance of 2.916 \AA , in very good agreement with the SW potential, but they obtain a dissociation energy of 22.9 kJ mol^{-1} , and estimate that the true value is at least 21 kJ mol^{-1} , which is larger than the SW energy.

3.6. Transition structures for the water dimer

It is desirable to test the reliability of the SW potential by monitoring its performance at regions of configuration space away from the minimum. In this respect, a comparison can usefully be made with the *ab initio* results of Smith *et al.* [71], who optimized the structures of ten stationary points on the water dimer surface, at the MP2 level, and calculated MP2 and MP4 energies for each point. Millot and Stone have also published a comparison of their ASP potential [65] with the results of Smith *et al.*, and found a slightly different energy ordering of the ten points. These results will also be compared here with the SW potential.

It should be noted that the results of Smith *et al.* include intramolecular degrees of freedom, whereas the SW potential assumes that the water molecules are rigid. In principle, the SW potential can be applied to water monomers in any intramolecular geometry, since the positions of the nuclei completely define the potential. In practice, it should only be used, in its current form, for rigid water molecules. The water charge densities, multipoles, polarizabilities and dispersion energy coefficients will change with monomer geometry, and this has not been included in the SW potential; even

Table 4. Calculated energies of various stationary points on the potential energy surface of the water dimer. The structures and labelling of the stationary points 1–10, and the MP2 and MP4 energies, are taken from [71]. MP2 and MP4 energies in parentheses are calculated using a larger basis set. Results for the ASP potential are taken from [65]. All energies are expressed as $-E/\text{kJ mol}^{-1}$.

Label	Number of H bonds	MP2 energy	MP4 energy	SW energy (this work)	ASP energy
1	1	27.0 (22.7)	22.4 (22.6)	19.8	18.2
2	1	24.3 (20.2)	19.6 (20.1)	17.5	14.3
3	1	24.2	19.3	17.2	14.1
4	2	21.9 (19.0)	18.2 (19.0)	18.5	16.5
5	2	20.7	16.9	17.7	13.6
6	2	20.6	16.7	17.5	13.8
7	3	17.8	14.7	15.6	15.3
8	4	8.5	6.7	6.8	7.3
9	2	19.8 (14.5)	14.9 (14.7)	15.7	14.2
10	2	14.3	10.6	11.2	10.4

more importantly, the change in intramolecular potential with monomer distortion is not included. This should be borne in mind when comparing the SW and the *ab initio* results.

In table 4, the MP2 and MP4 energies of Smith *et al.* are reproduced, together with the SW and ASP [65] energies at the same geometries. Several of the energies have been recalculated by Smith *et al.* using a larger basis set, and these results are also given. The basis set superposition errors have been estimated by Smith *et al.* to be between about 15% and 20% of the intermolecular potential, at the MP4 level, and the use of a counterpoise correction would make all the results of Smith *et al.* correspondingly less negative.

Considering the uncertainty in the *ab initio* results, the agreement with the SW potential is very good. In all cases, the difference between the *ab initio* MP4 and SW energies is less than 12%, and changing the basis set does not substantially change the agreement. In contrast, the less accurate MP2 energies are all much more negative than the MP4 and SW results, up to 40% in some cases, but improving the basis set brings the MP2 energies closer to the others. The ASP potential is shallower than the SW potential, and differs from the *ab initio* results by 20–30% for structures 1, 2 and 3. These are the singly hydrogen-bonded stationary points, and are also the ones for which the SW potential differs most from the *ab initio* energies. It is perhaps significant that the difference between the SW and *ab initio* results always lies between 11% and 12% for structures 1–3, but for the multiply hydrogen-bonded structures the difference is 6% or less. The SW potential energy is also more negative than the *ab initio* energy for structures 4–10, whereas for structures 1–3 the reverse is the case. This means that the energy of multiply hydrogen-bonded dimers 4–10 is more favourable, relative to dimers 1–3, for the SW potential than for the *ab initio* calculations, but the energy ordering within each of the two groups is largely unchanged. The relative stabilization of structures 4–10 is about 3 kJ mol⁻¹ for the SW potential compared with the *ab initio* calculations, and is sufficient to make structures 4–6 lower in energy than structures 2 and 3 for the SW potential. A similar trend is observed for the ASP potential. There is evidently some systematic error, either in the SW and ASP potentials, or in the *ab initio* calculations (or both) that affects the singly and multiply hydrogen-bonded

structures differently. This is unlikely to be the neglect of charge transfer in the SW and ASP potentials, since Millot and Stone found that including charge transfer would stabilize the multiply hydrogen-bonded structures even more [65]. It also seems unlikely that the overlap model for the repulsion energy, used in the SW potential, is responsible for the errors, since the ASP potential used *ab initio* calculations of the repulsion energy. One possible source of error in the calculations of Smith *et al.* is the BSSE, which they estimate [71] to be about 1 kJ mol⁻¹ more for structures 1 and 2 than for structures 4 and 9. Removal of the BSSE would therefore improve the agreement with the model potentials, but a substantial discrepancy would still remain.

The prediction that transition structure 4 has the lowest energy is in agreement with the most recent experimental results of Karyakin *et al.* [81]. They predicted a barrier of 405 cm⁻¹ for the donor–acceptor interchange in the D₂O dimer, and 592 cm⁻¹ for the acceptor–acceptor interchange, and gave similar predictions for the H₂O dimer. This contrasts with earlier work and also with the results of Smith *et al.* [71], who predicted that the acceptor–acceptor interchange would have the lowest barrier. Although the barrier heights for the SW potential are much lower (about 100 cm⁻¹ for the donor–acceptor interchange) this agreement is quite pleasing, and suggests that the SW potential could serve as a starting point for fitting to spectroscopic data.

4. The non-additive potential

In the presence of an ion, the charge densities of water molecules are distorted, and the water–water interaction is modified, so the total potential in ion–water clusters is non-additive. This also occurs to a lesser extent in pure water. Many physical effects contribute to non-additive potentials. Even for the simplest case, three spherical atoms, a number of these contributions are significant, as has been discussed by Meath and Aziz [82]. For three non-spherical molecules, the situation is even more complicated. It is useful to distinguish between Coulomb, exchange and mixed contributions, and the relative importance of each of these types of contribution is considered here for small ion–water clusters.

Non-additive Coulomb contributions include the non-additive dispersion energy (including the Axilrod–Teller triple-dipole energy) and the induction energy. For Na⁺(H₂O)₂, the non-additive dispersion energy falls off asymptotically as $R_{AB}^{-3} R_{AC}^{-3} R_{BC}^{-3}$, with a small coefficient, and can be neglected. On the other hand, the component of the non-additive induction energy that describes the interaction of the dipole on one water molecule (B), induced by the ion (A), with the permanent dipole on another water molecule (C), is proportional to $R_{AB}^{-2} R_{BC}^{-3}$, and makes a significant contribution to the potential. The work of Chałasiński *et al.* on H₂O, HCl and HF trimers [83, 84] also has shown that the non-additive dispersion energy is negligible, and that the ‘deformation’ energy (which includes the induction energy) dominates the non-additive energy; these differences will be even greater when one of the molecules is replaced by an ion.

The model potential developed in this work therefore includes a non-additive induction energy. The field at each oxygen nucleus, due to the atom-centred charges and dipoles (from table 1) on the other water molecules and the ion, is calculated, and the field gradient at each oxygen nucleus is calculated from the permanent charges only, to be consistent with the water dimer potential of section 3. Each contribution to the field (or field gradient) is also damped by the square root of the appropriate energy damping function given in section 2.3 (ion–water) or 3.2 (water–water), as described in section 3.3. This is also consistent with the pair potentials, and is a reasonable

attempt to incorporate non-additivity into damping functions. The second-order induction energy is then given by

$$E_{\text{ind}}^{(2)} = -\frac{1}{2} \sum_A \sum_{lm, l'm'} F_{lm}^A F_{l'm'}^A \alpha_{mm'}^{ll'} \quad (36)$$

This includes both additive and non-additive terms, so it incorporates equations (8) and (27), which therefore are not used explicitly in the final model potential. A third-order contribution is also included, to describe the interaction of induced multipole moments due to the field of the ion.

$$E_{\text{ind}}^{(3)} = \sum_{A < B} \sum_{lm, l'm'} \sum_{LM, L'M'} F_{lm}^A(\text{ion}) \alpha_{mm'}^{ll'} F_{LM}^B(\text{ion}) \alpha_{MM'}^{LL'} T_{l'm', L'M'}^{\text{AB}}(R_{\text{AB}}, \Omega_{\text{AB}}), \quad (37)$$

where $F_{lm}^A(\text{ion})$ are the field and field gradient components at oxygen nucleus A produced by the charge of the ion. Contributions to the electric field due to other water molecules are neglected in the third-order energy. There are three reasons for this: first, it makes simulations of ion–water clusters easier to perform, as they require no iteration of the induction energy, and moving one water molecule requires only of order N operations to recalculate the energy (N is the number of water molecules); second, in relatively small clusters the contribution from the ion dominates the electric field, since at a given water molecule the field of the ion is about ten times stronger than the field of other water molecules; third, the absence of a specific third-order energy for pure water is most consistent with the water pair potential used.

Other contributions to the non-additive potential include the effects of electron exchange. For example, the Heitler–London energy for the cluster, which is the expectation energy calculated using the ground-state monomer wavefunctions antisymmetrized over all electron coordinates, contains some non-additive terms. These include a first-order three-body exchange energy, which occurs even for three spherical atoms, and the interaction of exchange-induced multipoles on two molecules with the permanent multipoles of a third, which can be classified as a mixed Coulomb–exchange term. The three-body exchange behaves asymptotically approximately as $\exp(-\alpha R_{\text{AB}} - \beta R_{\text{AC}} - \gamma R_{\text{BC}})$, and the mixed term as $\exp(-\alpha R_{\text{AB}}) R_{\text{AC}}^{-n}$, where the smallest value of n is 2 for the ion–water–water trimer. For large separations, these exchange and mixed contributions are insignificant, but for nearest neighbours they may be important. The development of models to describe these effects is still at a very early stage [85, 86], and they are likely to be less important than the non-additive induction energy. In particular, the non-additive Heitler–London energy is found to be less important than the induction energy for the trimers considered by Chałasiński *et al.* [83, 84], and this will also be true for trimers including an ion. Non-additive exchange effects are neglected in the current work.

5. Simulations of $\text{Na}^+(\text{H}_2\text{O})_N$, $N = 1-6$

Solvation of a sodium ion by a small number of water molecules is simulated using a classical Monte Carlo algorithm, with importance sampling, at a constant temperature $T = 298$ K. The ion is fixed at the origin of coordinates, and initially N water molecules are placed randomly around it. The cluster is equilibrated by making $10000N$ attempted molecular moves, then $30000N$ further moves are attempted, during which statistical information is collected. For $N = 1$, it is estimated visually that about 400 attempted moves are required to remove correlations in the cluster energy, and this increases to about 1600 attempted moves for $N = 6$. Standard errors

in the average quantities are therefore multiplied by between 20 (for $N = 1$) and 40 (for $N = 6$). To avoid the unphysical short range maxima in the potentials, hard spheres with diameter $2.5 a_0$ are placed on the nuclei. In practice, this short internuclear separation is never approached in the simulations.

Attempted molecular moves are performed by randomly selecting a molecule, translating it by up to $0.5 a_0$ in a random direction, then rotating it by up to 0.15 rad about a random axis passing through the oxygen nucleus. The attempted move is accepted if $\exp(-\Delta E/kT) > R$, where R is a uniformly distributed random number in the range $0-1$, and ΔE is the change in potential energy of the cluster caused by the attempted move. Each attempted move is an order N process, requiring recalculation of $N-1$ water-water pair potentials, one water-ion potential, $2N-1$ field and field gradient contributions, N contributions to the second-order induction energy and $N-1$ contributions to the third-order induction energy.

To calculate the free energy change for the complexation reaction



a thermodynamic perturbation method is used [44, 45]. One of the water molecules is 'labelled', and the potential energy $E_N - E_{\text{H}_2\text{O}}$ of the $\text{Na}^+(\text{H}_2\text{O})_{N-1}$ cluster without the labelled molecule is calculated, as well as E_N , the potential energy of the $\text{Na}^+(\text{H}_2\text{O})_N$ cluster. For 100 values of a parameter λ , given by $\lambda_k = [(k-0.5)/100]^2$, $k = 1-100$, an attempted move is accepted if $\exp(-\Delta W/kT) > R$, where W is defined by

$$W = E_N - E_{\text{H}_2\text{O}} + \lambda(E_{\text{H}_2\text{O}}). \quad (39)$$

When $\lambda \approx 0$, the position of the labelled molecule has almost no effect on the sampling, and it behaves as an ideal gas molecule. It is confined, in the simulation, by a box of volume $V_c = 33510 a_0^3$ centred on the ion. When $\lambda \approx 1$, the labelled molecule is essentially fully bound to the cluster. Two simulations are performed for each N , one with λ increasing from 0 to 1 and one with λ decreasing from 1 to 0; no systematic difference is found. The complexes are equilibrated for 50 000 attempted moves at the starting value of λ , and for 1000 attempted moves for each subsequent value. Statistical averages are calculated over a further 1000 attempted moves for each λ . Each attempted move is again an order N process. To improve the sampling, attempted translations and rotations of the labelled molecule are a factor of $\lambda^{-1/2}$ larger than for the unlabelled molecules, but not larger than $10 a_0$ and 3 rad, respectively. Every 100 attempted moves, an attempt is made to exchange the position of the labelled molecule with a randomly chosen unlabelled molecule. This attempt is successful if $\exp(-\Delta W/kT) > R$, where ΔW is the change in W caused by exchanging the molecules.

5.1. Complexation enthalpies and free energies

The enthalpy of complexation for reaction (38) is obtained from the Monte Carlo simulations of $\text{Na}^+(\text{H}_2\text{O})_N$ and $\text{Na}^+(\text{H}_2\text{O})_{N-1}$, using [44]

$$\Delta H = \langle E_N \rangle - \langle E_{N-1} \rangle - kT, \quad (40)$$

where $\langle E_N \rangle$ is the average potential energy of $\text{Na}^+(\text{H}_2\text{O})_N$, and $\langle E_0 \rangle = 0$. The free energy of complexation is obtained from the thermodynamic perturbation results,

$$\Delta G = \int_0^1 \langle E_{\text{H}_2\text{O}}(\lambda) \rangle d\lambda + kT \ln N + kT \ln (V_m/V_c) - kT, \quad (41)$$

where $V_m = 277655 a_0^3$ is the volume of a free gas molecule at $T = 298$ K. The integral

is transformed to an integral over $\lambda^{1/2}$, and evaluated using the trapezium rule. The results are compared with information from mass spectrometry [40, 87] and collision-induced dissociation experiments [41] in table 5.

The free energy changes are in good agreement with experiment, especially for larger clusters, but they are more negative than the free energies obtained by Džidić and Kebarle [40] from mass spectrometry for $N = 1 \rightarrow 2$ and $N = 2 \rightarrow 3$. This is also the case for the enthalpy change in these processes, and suggests a possible deficiency in the non-additive potential. However, the bond energies obtained more recently by Dalleska *et al.* [41], using collision induced dissociation of the clusters with xenon atoms, are more negative than comparable energies obtained from mass spectrometry. If these differences were retained in the free energies and enthalpies, there would be no disagreement with this experiment, within the quoted uncertainties. For the larger clusters, the enthalpy changes are calculated to be less negative than the results obtained from mass spectrometry, but only for $N = 5 \rightarrow 6$ is the enthalpy outside the error bounds. The free energy change differs from the experimental result in the opposite direction, and is within the experimental bounds.

Results are also shown in the table for the modified RWK2 potential of Lybrand and Kollman [88], which consists of the water potential of Reimers *et al.* [89] plus polarizability, and ion–water potential and non-additivity fitted to the $N = 0 \rightarrow 1$ and $N = 1 \rightarrow 2$ enthalpies; the POL1 potential of Caldwell *et al.* [50]; the TIP4P potential of Jorgensen *et al.* [90] with the ion–water potential of Chandrasekhar *et al.* [91]; and the *ab initio* potentials (denoted KPC here) of Kistenmacher *et al.* [43] for $\text{Na}^+\text{-H}_2\text{O}$ and Lie and Clementi [92] for $\text{H}_2\text{O}\text{-H}_2\text{O}$. The results are taken from simulations performed by Cieplak *et al.* [93] (RWK2), Dang *et al.* [94] (POL1), Perera and Berkowitz [95] (TIP4P, POL1), Jorgensen and Severance [96] (TIP4P), and Mruzik *et al.* [44] (KPC).

The RWK2 and POL1 models, which were fitted to data for both $N = 0 \rightarrow 1$ and $N = 1 \rightarrow 2$, show discrepancies from experiment in the same direction as the current SII/SW potential for $N = 2 \rightarrow 3$. For larger N , the POL1 potential seems to give enthalpies that are closest to the SII/SW potential, but all the simulation results become less precise for $N > 4$. The KPC *ab initio* potential produces energies that are much too negative, as a result of the low level of *ab initio* theory and the neglect of the non-additive potential, and the TIP4P results are also too negative for clusters up to $\text{Na}^+(\text{H}_2\text{O})_4$. For larger clusters, the TIP4P results are surprisingly in much better agreement with experiment. There is a possibility that the experimental enthalpies are themselves too negative for $N = 4 \rightarrow 5$ and $N = 5 \rightarrow 6$: it seems unlikely that the TIP4P potential would abruptly start to give better results for larger clusters than the RWK2 potential and the current potential. Furthermore, the close agreement of the current potential with the experimental free energy suggests a discrepancy between the experimental free energy and enthalpy values. More accurate experimental measurements of these thermodynamic quantities are required to differentiate better between the various potentials, but the current potential seems to be at least as accurate as any of other potentials considered.

5.2. Structure and energetics of the solvation shell

When $N \leq 4$ water molecules are added to a gas-phase sodium ion, they arrange themselves around the ion at approximately the optimum $\text{Na}^+\text{-H}_2\text{O}$ geometry, with Na–O distances of around $4.2 a_0$, and hydrogen atoms pointing outwards, while the

Table 5. Comparison of calculated and experimental enthalpies and free energies for the complexation reaction $\text{Na}^+(\text{H}_2\text{O})_{N-1} + \text{H}_2\text{O} \rightarrow \text{Na}^+(\text{H}_2\text{O})_N$ at 298 K. Experimental data (Exp) are taken from [40] and [87], SW refers to the current work, and other results are taken from the references in the text. Figures in parentheses are uncertainties in the final digit; the uncertainties in the experimental data are estimated to be between 4 and 8 kJ mol⁻¹.

N	Exp	SW	RWK2	POL1	TIP4P	KPC
Enthalpies, $-\Delta H/\text{kJ mol}^{-1}$						
1	100 ^a	100 (0)	101 (0)	101 (2)	100 (0)	104 (0)
2	83 ^a	88 (1)	89 (0)	84 (3)	93 (0)	97 (0)
3	66 ^a	72 (1)	77 (1)	72 (3)	83 (0)	85 (1)
4	58 ^a	56 (1)	65 (1)	54 (4)	72 (0)	74 (1)
5	51	45 (2)	43 (2)	44 (4), 50 (9)	50 (0)	62 (2)
6	45	35 (2)	41 (3)	53 (5), 43 (9)	45 (1)	53 (4)
Free energies, $-\Delta G/\text{kJ mol}^{-1}$						
1	74 ^a	74 (1)				78 (0)
2	55 ^a	61 (1)				67 (1)
3	39 ^a	44 (1)				55 (1)
4	26 ^a	30 (1)				42 (1)
5	16	19 (1)				31 (2)
6	12	15 (1)				24 (1)

^a Collision-induced dissociation experiments [41] have been interpreted to give energies that differ from the tabulated results as follows: $N = 1$, no difference; $N = 2$, 2 kJ mol⁻¹ deeper; $N = 3$, 7 kJ mol⁻¹ deeper; $N = 4$, 1 kJ mol⁻¹ shallower.

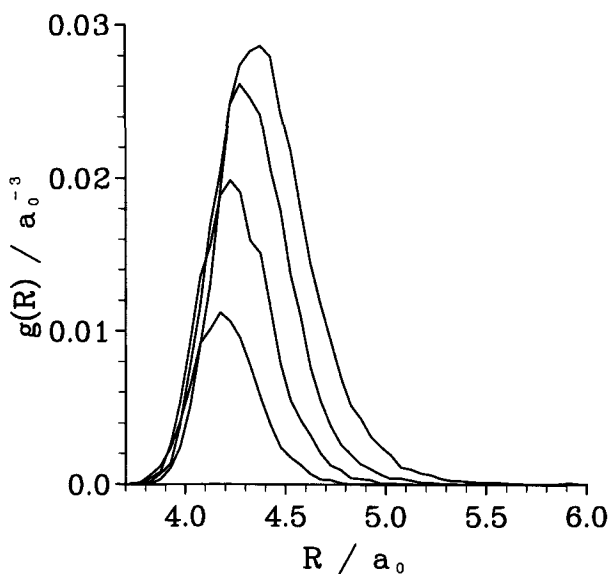


Figure 4. Ion-oxygen radial distribution functions $g(R)$ for $\text{Na}^+(\text{H}_2\text{O})_N$, $N = 1-4$, normalized so that $\int_0^\infty 4\pi R^2 g(R) dR = N$.

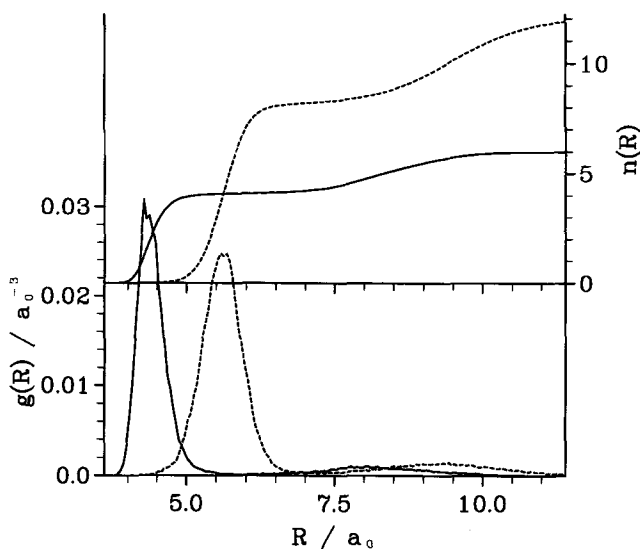


Figure 5. Ion-oxygen (solid line) and ion-hydrogen (dashes) radial distribution functions $g(R)$ for $\text{Na}^+(\text{H}_2\text{O})_6$. The integrated radial distribution functions $n(R)$ are defined by $n(R) = \int_0^R 4\pi R^2 g(R) dR$.

water molecules keep as far away from each other as possible. The cluster is therefore approximately linear for $N = 2$, equilateral for $N = 3$ and tetrahedral for $N = 4$. The Na-O radial distribution functions, obtained from the Monte Carlo cluster simulations, are shown in figure 4 for $N = 1-4$. As N increases, the most common Na-O distance increases by about $0.1-0.2 a_0$, mostly from $N = 3$ to $N = 4$, and the maximum distance from the ion at which water molecules can be found increases more steadily and substantially, by about $0.2 a_0$ per water molecule added. This shows that the water molecules in the solvation shell repel each other, as expected.

The fifth and sixth water molecules start a new solvation shell, because it is energetically unfavourable to pack any more water molecules closely around the ion. The Na-O and Na-H radial distribution functions are shown in figure 5 for $N = 6$, with the integrated distribution function $n(R)$ giving the number of O (and H) nuclei on average within a distance R of the ion. Although the scale is different, the Na-O distribution function is closely similar to the distribution function for $N = 4$, for R up to about $6 a_0$. The remaining two water molecules are seen to remain outside this solvation shell. The Na-H radial distribution function has a similar shape to the Na-O distribution, but shifted further from the ion, showing that the hydrogen atoms tend to point away from the ion in the second as well as the first solvation shell. It should be noted that neither distribution function actually drops to zero between the first and second solvation shells, suggesting that molecules are exchanged freely between the solvation shells. This phenomenon was, in fact, observed in the simulations for both $N = 5$ and $N = 6$.

In figure 6, the distribution of $\text{Na}^+-\text{H}_2\text{O}$ pair energies is shown for $N = 1-6$. These exclude the induction energy, which is fundamentally a non-pairwise-additive quantity, and are therefore always less negative than the minimum of the S11 $\text{Na}^+-\text{H}_2\text{O}$ potential. The first maximum occurs at similar energies for all six clusters, although it is interesting that the height of the first peak does not increase from $N =$

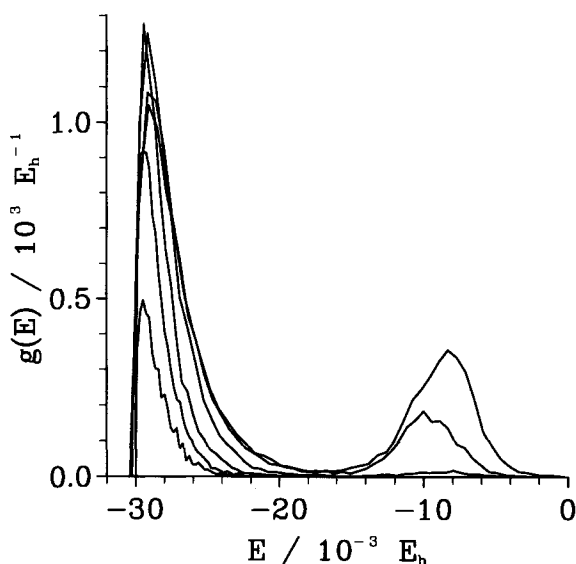


Figure 6. Distribution of $\text{Na}^+\text{-H}_2\text{O}$ pair energies for $\text{Na}^+(\text{H}_2\text{O})_N$, $N = 1\text{-}6$, normalized so that $\int_{-\infty}^{\infty} g(E) dE = N$. The peak around $E = -29 \times 10^{-3} E_h$ increases in height along the sequence $N = 1, 2, 6, 5, 4, 3$; the peak around $E = -9 \times 10^{-3} E_h$ is not observed for $N = 1\text{-}3$, and increases in height from $N = 4$ to $N = 6$.

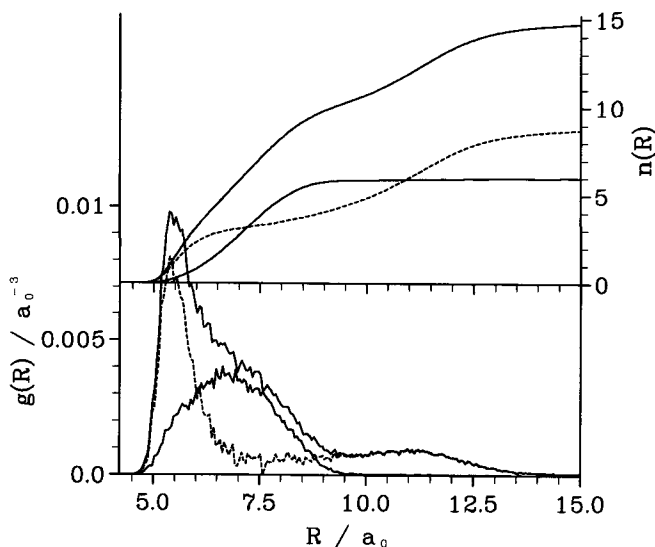


Figure 7. Oxygen–oxygen radial distribution functions $g(R)$, and integrated radial distribution functions $n(R)$, for $\text{Na}^+(\text{H}_2\text{O})_4$ (lower solid lines) and $\text{Na}^+(\text{H}_2\text{O})_6$ (upper solid lines). The difference between $N = 4$ and $N = 6$ is shown as dashes.

3 to $N = 4$, and decreases from $N = 4$ to $N = 5$ and 6. This shows that water–water repulsion within the first solvation shell is sufficiently large for $N = 4$ that it can be favourable for the molecules to move out to slightly greater distances from the ion, where the ion–water potential is smaller; this effect was seen also in the shifting of the

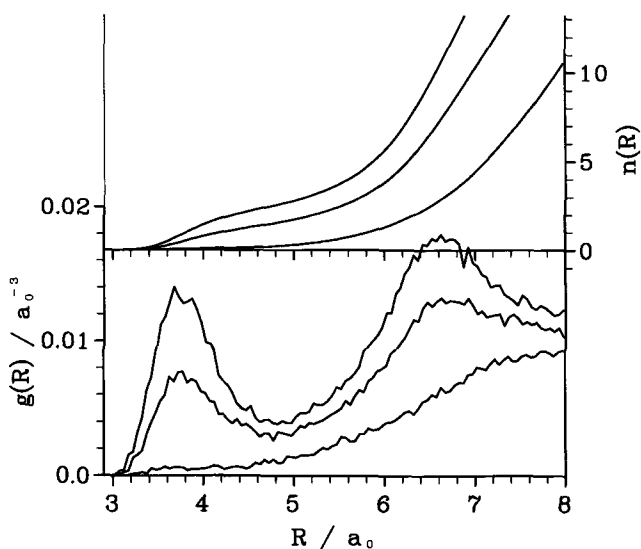


Figure 8. Oxygen-hydrogen radial distribution functions $g(R)$, and integrated radial distribution functions $n(R)$, for intermolecular contacts in $\text{Na}^+(\text{H}_2\text{O})_N$, $N = 4-6$. The normalization is $\int_0^\infty 4\pi R^2 g(R) dR = 2N(N-1)$.

peak in figure 4. For $N = 5$ and $N = 6$, it is possible that the water molecules in the first solvation shell have to move away from the most favourable ion-water geometry in order to optimize their interaction with molecules in the second solvation shell. Molecules in the second solvation shell are still relatively tightly bound to the ion, as shown in figure 6. Although the binding energy in the second shell is only about one-third of the energy in the first shell, it is about 1.5 times larger than the depth of the water-water potential well.

The interaction between molecules in the first and second solvation shells is investigated in more detail in figures 7-9. Figure 7 shows the O-O radial distribution function for $N = 4$ and $N = 6$. For $N = 4$ a single, broad peak is observed, consistent with the proposed structure of the solvation shell as a floppy tetrahedron. The radial distribution function for $N = 6$ shows a similar feature, but there is an additional peak around $R = 5.5 a_0$, as well as some less interesting features at long range. A difference plot of the two functions shows the structure of the additional peak more clearly, and the integrated number of O-O contacts, $n(R)$, indicates that there are between two and three more of these short O-O distances in $\text{Na}^+(\text{H}_2\text{O})_6$ than in $\text{Na}^+(\text{H}_2\text{O})_4$. These observations are explained by hydrogen bonding between water molecules in the first and second solvation shells. The minimum O-O distance in the SW potential is $5.5 a_0$, which agrees with the position of the peak. A molecule in the second solvation shell might bond to only one molecule in the first shell, or it might bridge two first-shell molecules, making two hydrogen bonds which would presumably be distorted and have a smaller energy. Apparently both possibilities occur in the simulations, since there are more than two, but less than four, short O-O distances.

Figure 8 show the O-H radial distribution functions for $N = 4, 5$ and 6 , at small interatomic separations. For $N = 5$ and $N = 6$ there is a prominent peak at about $3.7-3.8 a_0$, which agrees with the minimum O-H hydrogen bond distance of $3.7 a_0$ for the SW potential. Integrating up to the first minimum, at $4.7 a_0$, gives a total of 0.2

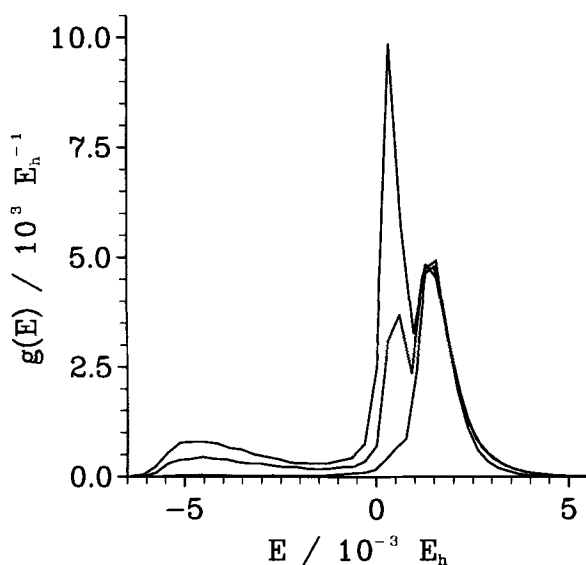


Figure 9. Distribution of $\text{H}_2\text{O}\text{-H}_2\text{O}$ pair energies for $\text{Na}^+(\text{H}_2\text{O})_N$, $N=4\text{-}6$, with the normalization $\int_{-\infty}^{\infty} g(E) dE = N(N-1)/2$. For $E < 10^{-3} E_h$, the bottom curve corresponds to $N=4$ and the top curve corresponds to $N=6$.

hydrogen bonds for $N=4$, 1.4 for $N=5$ and 2.4 for $N=6$. This supports the conclusion that neither the single nor the bridged hydrogen bonds are found exclusively. Figure 9 shows the distribution of $\text{H}_2\text{O}\text{-H}_2\text{O}$ pair energies, excluding the induction energy. There is a maximum around -5×10^{-3} , but the energy profile is relatively flat, showing that the hydrogen bonds are not rigid. This is to be expected at the temperature of the simulations, $T=298$ K. The area under the first peak, up to a fairly arbitrary energy cutoff $-1.5 \times 10^{-3} E_h$, gives 0.1 hydrogen bonds for $N=4$, 1.3 for $N=5$ and 2.4 for $N=6$, in good agreement with the previous estimate. It can also be seen from figure 9 that the water molecules predominantly repel one another when $N=4$, and the high-energy part of the figure is very similar for $N=4, 5$ and 6. This is further evidence for the relatively small effect of the fifth and sixth water molecules on the structure of the first solvation shell.

There has been some disagreement in the literature over the minimum-energy structure of $\text{Na}^+(\text{H}_2\text{O})_6$. The structure predicted by the current SI1/SW potential, with four molecules in the first solvation shell and two in the second shell, is supported by recent Hartree-Fock and MP2 *ab initio* calculations performed by Kim *et al.* [97], using the large Na^+ basis set of Bauschlicher *et al.* [47] plus a TZ2P water basis, and also by the MP2 calculations of Glendening and Feller [98], which were carried out with a smaller basis set. A density functional calculation previously had given an octahedral structure [99] for the cluster, and the simple model potential of Perez *et al.* [100] also suggested that a single solvation shell would be formed. It is noteworthy that even such 'coarse' details of ionic solvation are sensitive to the accuracy of the model potential (and the level of *ab initio* theory), and this shows the considerable importance of obtaining, and using, reliable intermolecular potentials when studying solvation processes.

6. Discussion

The systematic potentials developed in this work appear to be competitive with other published potentials, especially since only one parameter has been fitted for each pair interaction. For the water dimer, the structure and energy of the minimum are described to within experimental error, as are most of the second virial coefficient data. The nine other points on the water dimer surface considered here agree with supermolecule calculations to within basis set superposition error. For the $\text{Na}^+(\text{H}_2\text{O})_N$ clusters, the free energies and enthalpies of complexation agree with experimental results at least as well as other published potentials, although the error bounds are fairly large.

The S11 $\text{Na}^+\text{-H}_2\text{O}$ pair potential is expected to be one of the most accurate in the literature. The most important contributions to the binding energy are the ion-dipole and other electrostatic interactions, which are represented in detail using atom-centred multipoles, and the induction energy, which is modelled using accurate water polarizabilities. The repulsion energy depends on the shape of the electron density around the water molecule, and this is taken into account using large-basis-set SCF calculations of the charge densities of both water and Na^+ , which are built into the repulsion energy using a charge density overlap integral. Spectroscopic data on the $\text{Na}^+\text{-H}_2\text{O}$ dimer and related systems are now needed to provide the next advance in the accuracy of ion-molecule potentials; it is unlikely that supermolecule calculations will be competitive in the foreseeable future.

The SW water potential gives remarkably good agreement with experimental data, considering that only one parameter has been fitted. The least accurate part of the potential is likely to be the induction and dispersion energy damping functions, as discussed in section 3, but it is possible that the fitted parameter could absorb some of the deficiencies in these functions. It is expected that potentials constructed in this way, with relatively little reliance on experiment, will continue to be important in the future, even for interactions between small molecules. The water dimer illustrates this point well. Although it has been studied more widely than any other molecule-molecule interaction, except possibly the HF dimer, nothing specific is yet known about its potential energy surface, even the structure and energy at the minimum. Development of an accurate pair potential would require a fitting procedure using converged six-dimensional bound-state calculations, which are out of the range of current computational power. For example, the recent calculations of Althorpe and Clary [101, 102] were performed using an adiabatic separation of the radial motion from the five angular coordinates, within the coupled states approximation. This will introduce significant errors, of at least a few cm^{-1} , into the bound-state energies. Even with these approximations, the calculations could be used only to compare potentials, not to develop new ones. There is also the problem of intramolecular flexibility. The donor OH bond is expected to stretch significantly at the equilibrium geometry of the water dimer, and the HOH bond angle is likely to change in other geometries [71]. To account for these effects, a potential energy surface with 'rigid' water molecules, as in this work, must be fitted to experimental data for water molecules in their vibrational ground states, so the resulting potential can be interpreted as an adiabatic average over the intramolecular degrees of freedom. Different potentials could be envisaged for excited vibrational states, and different potentials would be required also for isotopically substituted water molecules. One problem is that potentials of this type are unable to describe coupling between intramolecular and intermolecular modes, as

for example in vibrational predissociation. Instead, a full twelve-dimensional potential energy surface could be calculated, including the intramolecular geometry explicitly. This potential energy surface could then be used for all isotopes of the water molecules. The systematic method is ideally suited to this, since it reduces the problem to three intramolecular degrees of freedom. However, accurate bound-state calculations using a twelve-dimensional potential would be far more difficult and expensive than six-dimensional calculations, so for most purposes the rigid molecule approach seems preferable.

The non-additive potential developed and used in this work is unlikely to be accurate, especially when there are four or more water molecules around the sodium ion. In the first solvation shell, the charge densities of the water molecules will be distorted by the field of the ion, which will affect the charge density overlap between neighbouring water molecules, and therefore change the repulsion energy. This effect has not been taken into account in the models; it is part of the 'deformation' energy calculated by Chałasiński *et al.* [83, 84]. The available experimental data are not sufficient to fit accurate non-additive potentials for $\text{Na}^+(\text{H}_2\text{O})_N$, especially since the data contain contributions from both the pair potentials and the non-additive potentials, and errors in the (larger) pair potentials will tend to dominate. Supermolecule calculations may be a better route for developing non-additive potentials in this case, in particular for modelling the polarization–repulsion (deformation) energy, since a significant contribution to this appears at the Hartree–Fock level.

The monomer properties required for the systematic potentials have been calculated from SCF wavefunctions, and could be improved using correlated *ab initio* calculations. It is preferable to use large-basis-set, Hartree–Fock quality wavefunctions than correlated wavefunctions obtained using smaller basis sets, even though the variational energies for the Hartree–Fock monomers will be worse, because the small-basis-set wavefunctions will be quite inaccurate in the outer regions of the valence charge density, which are crucial in calculating the charge density overlap integrals and Coulomb energy integrals for the model potentials. However, since computer power is continually increasing, it is now becoming feasible to perform calculations with basis sets of similar size to those used in this work, using correlated *ab initio* methods. Even MP2 calculations could be useful: for example, they substantially reduce the error in the dipole moment of the water molecule [65]. The systematic method can be applied readily using correlated calculations, since only one calculation is required on each monomer.

Monte Carlo simulations have shown that gas-phase clusters consisting of a sodium ion with four to six water molecules have a first solvation shell containing four water molecules, and a second solvation shell containing the rest. This is unlikely to be true in solution, since replacing the surrounding vacuum with bulk water will increase the external pressure and force more water molecules into the first solvation shell. It appears that interchange of water molecules between the first solvation shell and the bulk will be rapid. More details on the structure and dynamics of ion solvation will be provided by larger simulations, consisting of hundreds of water molecules solvating a single ion; for this purpose, the systematic potentials developed in this work should prove to be highly suitable.

This work was funded by an Ordinary Research Fellowship from the Engineering and Physical Sciences Research Council. Fortran subroutines to evaluate the S11 and SW potentials are available from the author.

References

- [1] NESBITT, D. J., 1994, *Ann. Rev. phys. Chem.*, **45**, 367.
- [2] LEOPOLD, K. R., FRASER, G. T., NOVICK, S. E., and KLEMPERER, W., 1994, *Chem. Rev.*, **94**, 1807.
- [3] RAO, C. N. R., and PRADEEP, T., 1991, *Chem. Soc. Rev.*, **20**, 477.
- [4] HUTSON, J. M., 1990, *Ann. Rev. phys. Chem.*, **41**, 123.
- [5] SELEGUE, T. J., CABARCOS, O. M., and LISY, J. M., 1994, *J. chem. Phys.*, **100**, 4790.
- [6] MCKAY, R. I., BIESKE, E. J., ATKINSON, I. M., BENNETT, F. R., BRADLEY, A. J., RAINBIRD, M. W., ROCK, A. B., UICHANCO, A. S., and KNIGHT, A. E. W., 1990, *Aust. J. Phys.*, **43**, 683.
- [7] HABERLAND, H., v. ISSENDORFF, B., FRÖCHTENICHT, R., and TOENNIES, J. P., 1995, *J. chem. Phys.*, **102**, 8773.
- [8] OHASHI, K., and NISHI, N., 1991, *J. chem. Phys.*, **95**, 4002.
- [9] MARKOVICH, G., GINIGER, R., LEVIN, M., and CHESHNOVSKY, O., 1991, *Z. Phys.*, D, **20**, 69.
- [10] YEH, L. I., OKUMURA, M., MYERS, J. D., PRICE, J. M., and LEE, Y. T., 1989, *J. chem. Phys.*, **91**, 7319.
- [11] BOYS, S. F., and BERNARDI, F., 1970, *Molec. Phys.*, **19**, 553.
- [12] VAN DUJNEVELDT, F. B., VAN DUJNEVELDT-VAN DE RIJDT, J. G. C. M., and VAN LENTHE, J. H., 1994, *Chem. Rev.*, **94**, 1873.
- [13] MOROKUMA, K., 1971, *J. chem. Phys.*, **55**, 1236.
- [14] KITaura, K., and MOROKUMA, K., 1976, *Int. J. Quantum Chem.*, **10**, 325.
- [15] JEZIORSKI, B., MOSYNSKI, R., and SZALEWICZ, K., 1994, *Chem. Rev.*, **94**, 1887.
- [16] WHEATLEY, R. J., and PRICE, S. L., 1990, *Molec. Phys.*, **69**, 507.
- [17] WHEATLEY, R. J., and PRICE, S. L., 1990, *Molec. Phys.*, **71**, 1381.
- [18] SIEBERS, J. G., BUCK, U., and WHEATLEY, R. J., unpublished.
- [19] BEU, T. A., BUCK, U., SIEBERS, J. G., and WHEATLEY, R. J., unpublished.
- [20] WHEATLEY, R. J., and HUTSON, J. M., 1995, *Molec. Phys.*, **84**, 879.
- [21] AHLRICHS, R., PENCO, R., and SCOLES, G., 1977, *Chem. Phys.*, **19**, 119.
- [22] HEPBURN, J., SCOLES, G., and PENCO, R., 1975, *Chem. Phys. Lett.*, **36**, 451.
- [23] DOUKETIS, C., SCOLES, G., MARCHETTI, S., ZEN, M., and THAKKAR, A. J., 1982, *J. chem. Phys.*, **76**, 3057.
- [24] AZIZ, R. A., and SLAMAN, M. J., 1986, *Molec. Phys.*, **58**, 679.
- [25] TANG, K. T., and TOENNIES, J. P., 1977, *J. chem. Phys.*, **66**, 1496.
- [26] TANG, K. T., and TOENNIES, J. P., 1984, *J. chem. Phys.*, **80**, 3726.
- [27] NG, K.-C., MEATH, W. J., and ALLNATT, A. R., 1978, *Chem. Phys.*, **32**, 175.
- [28] NG, K.-C., MEATH, W. J., and ALLNATT, A. R., 1979, *Molec. Phys.*, **37**, 237.
- [29] DHAM, A. K., MEATH, W. J., ALLNATT, A. R., AZIZ, R. A., and SLAMAN, M. J., 1990, *Chem. Phys.*, **142**, 173.
- [30] AZIZ, R. A., SLAMAN, M. J., KOIDE, A., ALLNATT, A. R., and MEATH, W. J., 1992, *Molec. Phys.*, **77**, 321.
- [31] WHEATLEY, R. J., and MEATH, W. J., 1993, *Molec. Phys.*, **79**, 253.
- [32] PRICE, S. L., STONE, A. J., and ALDERTON, M., 1984, *Molec. Phys.*, **52**, 987.
- [33] STONE, A. J., 1981, *Chem. Phys. Lett.*, **83**, 233.
- [34] STONE, A. J., and ALDERTON, M., 1985, *Molec. Phys.*, **56**, 1047.
- [35] CLOUGH, S. A., BEERS, Y., KLEIN, G. P., and ROTHMAN, L. S., 1973, *J. chem. Phys.*, **59**, 2254.
- [36] WHEATLEY, R. J., and MITCHELL, J. B. O., 1994, *J. comput. Chem.*, **15**, 1187.
- [37] ZEISS, G. D., and MEATH, W. J., 1977, *Molec. Phys.*, **33**, 1155.
- [38] BARTOLOTTI, L. J., 1984, *J. chem. Phys.*, **80**, 5687.
- [39] WHEATLEY, R. J., and VIEHLAND, L. A., 1994, unpublished.
- [40] DŽIDIĆ, I., and KEBARLE, P., 1970, *J. phys. Chem.*, **74**, 1466.
- [41] DALLESKA, N. F., TIJLTA, B. L., and ARMENTROUT, P. B., 1994, *J. phys. Chem.*, **98**, 4191.
- [42] MCKNIGHT, L. G., and SAWINA, J. M., 1972, *J. chem. Phys.*, **57**, 5156.
- [43] KISTENMACHER, H., POPKIE, H., and CLEMENTI, E., 1973, *J. chem. Phys.*, **59**, 5842.
- [44] MRUZIK, M. R., ABRAHAM, F. F., SCHREIBER, D. E., and POUND, G. M., 1976, *J. chem. Phys.*, **64**, 481.
- [45] STRAATSMA, T. P., and BERENDSEN, H. J. C., 1988, *J. chem. Phys.*, **89**, 5876.
- [46] MAGNUSSON, E., 1994, *J. phys. Chem.*, **98**, 12558.

- [47] BAUSCHLICHER, C. W., LANGHOFF, S. R., PARTRIDGE, H., RICE, J. E., and KOMORNICKI, A., 1991, *J. chem. Phys.*, **95**, 5142.
- [48] ŠPIRKO, V., DAADOCH, N. M., JENSEN, H. J. A., JØRGENSEN, P., and HELGAKER, T., 1991, *Chem. Phys. Lett.*, **185**, 265.
- [49] DACRE, P. D., 1984, *Molec. Phys.*, **51**, 633.
- [50] CALDWELL, J., DANG, L. X., and KOLLMAN, P. A., 1990, *J. Amer. chem. Soc.*, **112**, 9144.
- [51] MITCHELL, J. B. O., and PRICE, S. L., 1989, *Chem. Phys. Lett.*, **154**, 267.
- [52] BUCKINGHAM, A. D., and FOWLER, P. W., 1985, *Can. J. Chem.*, **63**, 2018.
- [53] HURST, G. J. B., FOWLER, P. W., STONE, A. J., and BUCKINGHAM, A. D., 1986, *Int. J. Quantum Chem.*, **29**, 1223.
- [54] GLENDENING, E. D., and STREITWIESER, A., 1994, *J. chem. Phys.*, **100**, 2900.
- [55] STONE, A. J., 1993, *Chem. Phys. Lett.*, **211**, 101.
- [56] WHEATLEY, R. J., 1993, *Molec. Phys.*, **79**, 597.
- [57] STONE, A. J., 1978, *Molec. Phys.*, **36**, 241.
- [58] BRINK, D. M., and SATCHLER, G. R., 1968, *Angular Momentum*, 2nd Edn (Oxford: Clarendon Press).
- [59] DALGARNO, A., and DAVISON, W. D., 1966, *Adv. atomic molec. Phys.*, **2**, 1.
- [60] SINGH, T. R., and MEATH, W. J., 1971, *J. chem. Phys.*, **54**, 1137.
- [61] FIGARI, G., MUSSO, G. F., and MAGNASCO, V., 1985, *Molec. Phys.*, **54**, 689.
- [62] WORMER, P. E. S., and HETTEMA, H., 1992, *J. chem. Phys.*, **97**, 5592.
- [63] WHEATLEY, R. J., and MEATH, W. J., 1993, *Molec. Phys.*, **80**, 25.
- [64] FUCHS, R. R., MCCOURT, F. R. W., THAKKAR, A. J., and GREIN, F., 1984, *J. phys. Chem.*, **88**, 2036.
- [65] MILLOT, C., and STONE, A. J., 1992, *Molec. Phys.*, **77**, 439.
- [66] KELL, G. S., MCLAURIN, G. E., and WHALLEY, E., 1968, *J. chem. Phys.*, **48**, 3805.
- [67] EUBANK, P. T., JOFFRION, L. L., PATEL, M. R., and WAROWNY, W., 1988, *J. chem. Thermodyn.*, **20**, 1009.
- [68] KOZACK, R. E., and JORDAN, P. C., 1992, *J. chem. Phys.*, **96**, 3120.
- [69] CURTISS, L. A., FRURIP, D. J., and BLANDER, M., 1979, *J. chem. Phys.*, **71**, 2703.
- [70] DYKE, T. R., MACK, K. M., and MUENTER, J. S., 1977, *J. chem. Phys.*, **66**, 498.
- [71] SMITH, B. J., SWANTON, D. J., POPLÉ, J. A., SCHAEFER, H. F., and RADOM, L., 1990, *J. chem. Phys.*, **92**, 1240.
- [72] RYBAK, S., JEZIORSKI, B., and SZALEWICZ, K., 1991, *J. chem. Phys.*, **95**, 6576.
- [73] FELLER, D., 1992, *J. chem. Phys.*, **96**, 6104.
- [74] VAN DUINEVELDT-VAN DE RIJDT, J. G. C. M., and VAN DUINEVELDT, F. B., 1992, *J. chem. Phys.*, **97**, 5019.
- [75] SAEBØ, S., TONG, W., and PULAY, P., 1993, *J. chem. Phys.*, **98**, 2170.
- [76] CHAKRAVORTY, S. J., and DAVIDSON, E. R., 1993, *J. phys. Chem.*, **97**, 6373.
- [77] DANG, L. X., 1992, *J. chem. Phys.*, **97**, 2659.
- [78] WALLQVIST, A., and BERNE, B. J., 1993, *J. phys. Chem.*, **97**, 13841.
- [79] ÅSTRAND, P.-O., LINSE, P., and KARLSTRÖM, G., 1995, *Chem. Phys.*, **191**, 195.
- [80] FRANKEN, K. A., and DYKSTRA, C. E., 1994, *J. chem. Phys.*, **100**, 2865.
- [81] KARYAKIN, E. N., FRASER, G. T., and SUENRAM, R. D., 1993, *Molec. Phys.*, **78**, 1179.
- [82] MEATH, W. J., and AZIZ, R. A., 1984, *Molec. Phys.*, **52**, 225.
- [83] CHAŁASIŃSKI, G., SZCZĘŚNIAK, M. M., CIEPLAK, P., and SCHEINER, S., 1991, *J. chem. Phys.*, **94**, 2873.
- [84] CHAŁASIŃSKI, G., CYBULSKI, S. M., SZCZĘŚNIAK, M. M., and SCHEINER, S., 1989, *J. chem. Phys.*, **91**, 7048.
- [85] WHEATLEY, R. J., 1995, *Molec. Phys.*, **84**, 899.
- [86] COOPER, A. R., and HUTSON, J. M., 1993, *J. chem. Phys.*, **98**, 5337.
- [87] BANIC, C. M., and IRIBARNE, J. V., 1985, *J. chem. Phys.*, **83**, 6432.
- [88] LYBRAND, T. P., and KOLLMAN, P. A., 1985, *J. chem. Phys.*, **83**, 2923.
- [89] REIMERS, J. R., WATTS, R. O., and KLEIN, M. L., 1982, *Chem. Phys.*, **64**, 95.
- [90] JØRGENSEN, W. L., CHANDRASEKHAR, J., MADURA, J. D., IMPEY, R. W., and KLEIN, M. L., 1983, *J. chem. Phys.*, **79**, 926.
- [91] CHANDRASEKHAR, J., SPELLMEYER, D. C., and JØRGENSEN, W. L., 1984, *J. Amer. chem. Soc.*, **106**, 903.
- [92] LIE, G. C., and CLEMENTI, E., 1975, *J. chem. Phys.*, **62**, 2195.

- [93] CIEPLAK, P., LYBRAND, T. P., and KOLLMAN, P. A., 1987, *J. chem. Phys.*, **86**, 6393.
- [94] DANG, L. X., RICE, J. E., CALDWELL, J., and KOLLMAN, P. A. 1991, *J. Amer. chem. Soc.*, **113**, 2481.
- [95] PERERA, L., and BERKOWITZ, M. L., 1991, *J. chem. Phys.*, **95**, 1954; erratum, 1993, *J. chem. Phys.*, **99**, 4236.
- [96] JORGENSEN, W. L., and SEVERANCE, D. L., 1993, *J. chem. Phys.*, **99**, 4233.
- [97] KIM, J., LEE, S., CHO, S. J., MHIN, B. J., and KIM, K. S., 1995, *J. chem. Phys.*, **102**, 839.
- [98] GLENDENING, E. D., and FELLER, D., 1995, *J. phys. Chem.*, **99**, 3060.
- [99] WAIZUMI, K., MASUDA, H., and FUKUSHIMA, N., 1993, *Inorg. Chim. Acta*, **209**, 207.
- [100] PEREZ, P., LEE, W. K., and PROHOFSKY, E. W., 1983, *J. chem. Phys.*, **79**, 388.
- [101] ALTHORPE, S. C., and CLARY, D. C., 1994, *J. chem. Phys.*, **101**, 3603.
- [102] ALTHORPE, S. C., and CLARY, D. C., 1995, *J. chem. Phys.*, **102**, 4390.